THESIS

# THE ROLE OF INTERNAL VARIABILITY AND EXTERNAL FORCING ON THE EMERGENCE OF COMPOUND EXTREMES IN THE CESM2 LARGE ENSEMBLE

Submitted by

Ashley E. Dwyer

Department of Atmospheric Science

In partial fulfillment of the requirements

For the Degree of Master of Science

Colorado State University

Fort Collins, Colorado

Summer 2025

Master's Committee:

Advisor: Elizabeth Barnes
Co-Advisor: James Hurrell

Frances Davenport

ABSTRACT

THE ROLE OF INTERNAL VARIABILITY AND EXTERNAL FORCING ON THE EMERGENCE OF COMPOUND EXTREMES IN THE CESM2 LARGE ENSEMBLE

Extreme hot and dry compound events pose significant hazards to human health, agriculture, and ecosystems, making it critical to better understand what drives their occurrence and spatiotemporal variability. Although the role of internal climate variability in driving compound events has been previously studied, we leverage a large ensemble to enable a more robust understanding of the response of hot and dry events to both large-scale internal climate variability and external forcing. We explore the influence of well-known large-scale climate modes including the El Niño Southern Oscillation (ENSO), Pacific Decadal Oscillation (PDO), Indian Ocean Dipole (IOD), and the North Atlantic Oscillation (NAO) on the occurrence of hot and dry compound events in the Community Earth System Model 2 Large Ensemble (CESM2-LE). We also investigate when anthropogenic changes in hot and dry compound events emerge from the noise of internal variability. Knowledge of drivers from an internal variability perspective combined with an understanding of greenhouse gas forced changes can aid in quantifying the predictability of extreme compound events on regional scales.

# ACKNOWLEDGEMENTS

I would like to thank my advisors Dr. Elizabeth Barnes and Dr. James Hurrell for their insight and mentorship during these last two years at Colorado State University, as well as Dr. Frances Davenport for serving on my graduate committee. I also would like to thank Kelsey Ennis, Dr. Martin Fernandez, and Charlotte Connolly for hearing out ideas and providing constructive comments throughout the development of this work. I thank the Barnes and Hurrell Research Groups for their camaraderie and mentorship. Lastly, thank you to all of my family, friends, and mentors (CSU, Loyola Maryland, and beyond) who have supported me.

The work in this thesis was supported by the National Science Foundation (grant no. AGS-2210068).

TABLE OF CONTENTS

# Chapter 1

# Introduction

Extreme weather and climate events have been studied for decades due to their effects on human health, agriculture, ecosystems, infrastructure, and the economy [1–3]. This research also includes what drives these events including internal variability such as large-scale internal climate modes [4] and external forcings such as anthropogenic climate change [5, 6]. For the former, recent work has demonstrated the utility of large ensemble models to study well-known large-scale climate modes as drivers of extreme events [7].

Large-scale climate modes including the El Niño Southern Oscillation (ENSO), Pacific Decadal Oscillation (PDO), Indian Ocean Dipole (IOD), and the North Atlantic Oscillation (NAO), are characterized by positive, neutral, and negative phases. The oscillating behavior of these four modes impacts temperature and precipitation in different regions and can thus influence the occurrence of extremes [8, 9]. Knowledge of the influence of these drivers on extreme events, including compound events, assists in the prediction of, and preparation for these events [10].

Compound events are hazards that occur in some combination including at the same time or sequentially [11]. The IPCC Special Report on Managing Risks of Extreme Events and Disaster to Advance Climate Change Adaptation (SREX) published in 2012 drew attention to the need to study compound events due to increased consequences of these events compared to extremes that occur individually [12]. Since the publication of the SREX, more studies have been devoted to understanding frequency changes of these extremes both in the historical period [13, 14] and under different future projections [15–17]. From this research, there is now growing evidence that anthropogenic climate change is impacting compound events due to its effects on temperature and precipitation. This thesis investigates extreme hot and dry events that occur at the same time and place (i.e. hot and dry compound events).

In chapter 2 of this thesis, we expand on previous literature by leveraging a large ensemble to provide a comprehensive analysis on the influence of four well-known climate modes on hot

and dry compound events at a global scale. This increases understanding of these events to unforced, internal climate variability, especially for regions, including South America and Africa, that are underrepresented in the existing literature [18]. Although frequencies of compound events are increasing in most regions, the idea of emergence of the events remains underexplored. We investigate when hot and dry compound events emerge from internal variability, building fundamental knowledge of when certain regions will see an influence from external forcing. We use 100 members from the Community Earth System Model version 2 Large Ensemble [19, 20] to investigate these two ideas. Using a large ensemble to analyze the roles of internal variability and external forcing on driving hot and dry compound events could aid in quantifying changes and predictability on regional scales.

Chapter 2, alongside the Appendix A as supplementary material, will be submitted as the following paper.

- Dwyer, A.E., Barnes, E.A., Hurrell, J.W. The Role of Internal Variability and External Forcing on the Emergence of Hot and Dry Compound Events in a Large Ensemble. *To be Submitted*

Chapter 3 describes possible future directions for research.

# Chapter 2

# The Role of Internal Variability and External Forcing on the Emergence of Compound Extremes in the CESM2 Large Ensemble

## 2.1 Introduction

Hot and dry compound events pose significant hazards through impacts on human health (e.g. temperature-related deaths), agriculture (e.g. reduction in crop yield), and ecosystems [21–23], making it critical to better understand what drives their occurrence and spatiotemporal variability. Although drivers of compound events, including and most often the El Niño Southern Oscillation (ENSO) [18], have been analyzed through the observational record [9, 24], recent work demonstrates the utility of large climate ensembles to advance physical understanding of the events drivers [7, 25, 26]. For example, Reddy et al. (2022) leveraged a large ensemble to quantify which combinations of ENSO and the Indian Ocean Dipole (IOD) phases have the greatest influence on compound events in Australia [25].

Numerous studies have examined how the variability, amplitude, and teleconnections of large-scale climate modes may be altered by anthropogenic climate change in the 21st century [27–29]. Such changes may lead to changes in extreme event occurrence in the future [30, 31]. Studies have also shown that the frequency of hot and dry compound events are changing due to the response of temperature and precipitation under climate change [13, 14, 17, 32]. Quantifying when changes in the frequency of hot and dry compound events may emerge from the noise of internal variability has primarily been analyzed in reanalysis and observational datasets. For example, Scmutz et al. (2025) analyzed the year of emergence in ECMWF version 5 reanalysis data [33] across Europe and northern Africa and found that, in most locations, compound events emerge from internal variability by 2015 [34]. Although observational and reanalysis datasets provide crucial insight on

historical patterns, large ensemble datasets, when compared to the short duration of observations and reanalysis products, increase the power of analyzing extreme events and allow for more robust assessments of future changes in compound event frequency.

Our study builds on the aforementioned literature by using a large climate model ensemble to analyze the influence of four different internal climate modes on compound events at a global scale. Leveraging a large ensemble enables a more robust understanding of the response of these events to both unforced and forced climate variability across the historical record in addition to the 21st century. We strive to expand understanding of the influence of large-scale patterns of internal climate variability on hot and dry compound events. After removing the external forcing signal, we explore how well-known large-scale climate modes including El Niño Southern Oscillation (ENSO), Pacific Decadal Oscillation (PDO), Indian Ocean Dipole (IOD), and the North Atlantic Oscillation (NAO) influence hot and dry compound events. We use the Community Earth System Model 2 Large Ensemble (CESM2-LE), which is a set of 100 historical and future climate simulations under SSP 3-7.0 [19, 20]. We then investigate how conditional frequencies of compound events are changing over the 21st century and compare this to the historical period. This builds on previous research on changing climate mode variability by analyzing its impact on future compound events. We then retain the external forcing component and investigate when hot and dry compound events emerge beyond the range of internal variability in the CESM2-LE.

## 2.2 Data and Methods

### 2.2.1 Data

We employ the CESM2-LE to study hot and dry compound events across preindustrial, present and future climates [19, 20]. CESM2-LE follows protocols provided by the Coupled Model Intercomparison Project Phase 6 (CMIP6), with historical forcings for 1850-2014 and SSP3-7.0 forcings for 2014-2100 [35]. Monthly data for precipitation rate (PRECT), 2m temperature (TREFHT), surface temperature (TS), and surface-level pressure (PSL) are used to define and analyze compound events on a 0.94° by 1.25° horizontal grid. The ensemble mean over all 100 members is

computed monthly and subtracted from each member to remove the forced response and the seasonal cycle. Temperature and precipitation anomalies are then analyzed for each month of every year from 1850 to 2100.

Monthly El Niño Southern Oscillation (ENSO), Indian Ocean Dipole (IOD), and Pacific Decadal Oscillation (PDO) indices from the Climate Variability Diagnostics Package [36, 37] are used to explore the connection between modes of internal climate variability and hot and dry compound events. Monthly North Atlantic Oscillation (NAO) indices are calculated in each member from the difference of normalized sea level pressure between Ponta Delgada, Azores (38.17 N, 25 W) and Stykkisholmur/Reykjavik, Iceland (63.61 N, 22.5 W) [38]. The positive phase of each of these four modes is defined as the anomalies in the indices that are $\geq$ 0.5, the negative phase as $\leq$ -0.5, and the neutral phase as the anomalies between these two bounds.

ECMWF Reanalysis V5 data [33] is used for comparison against the CESM2-LE results. Monthly 2m temperature (t2m), precipitation (tp; converted to a monthly rate), and surface temperature (skt) from ERA5 is analyzed from January 1940 through December 2023 after regridding to the CESM2-LE spatial grid using bilinear interpolation via the Climate Data Operators package [39]. We also use a 3rd order polynomial fit for each month and at every grid point to estimate and remove climate forcing and deseasonalize the ERA5 data to produce monthly anomalies.

### 2.2.2 Methods

We investigate multivariate extremes, or two hazards that occur in the same place at the same time [11]. The 90th percentile of monthly 2m temperature anomalies across the 100 members in the CESM2-LE is used to define extreme high temperatures. The 10th percentile of monthly precipitation rate anomalies across the 100 members is used to define extreme low precipitation. Concurrent hot and dry events (T90/P10) at a grid point thus occur when the monthly temperature anomaly exceeds the 90th percentile and the concurrent precipitation anomaly is below the 10th percentile. We investigate what drives compound events regardless of time of year; therefore, percentiles for each variable are computed for each month after combining the ensemble members.

In this way, anomalies from internal variability in specific seasons can be isolated and investigated (e.g. warm and dry extremes can occur in winter months and in wet seasons). A value of 1 is assigned to a gridpoint to signify a compound event in a given month, and a value of 0 is assigned if there is not a compound event. Analysis is then performed based on this binary classification. The global distribution of T90/P10 compound event frequencies are computed by averaging across all ensemble members over the 1850-1950 period. We then display the results as a percentage.

We compare our T90/P10 frequencies to independent frequencies, where temperature and precipitation variables are uncorrelated, to determine the extent to which internal variability is influencing the frequency of compound events. Independent frequencies are calculated via bootstrapping, where T90/P10 events are computed across scrambled ensemble members. Namely, the ensemble members for temperature are kept fixed and the ensemble members for precipitation are shifted down by one member (e.g. pairing temperature of member 1 with precipitation of member 2, temperature of member 2 with precipitation of member 3, etc.). The ensemble-mean frequencies across the 100 member pairings are then computed. We then proceed to shift the precipitation members again and run the same calculation. This is continued through the last possible combination. The result is 99 ensemble-mean frequencies under the null hypothesis of independent, uncorrelated variables. From here, we compute the 1st and 99th percentiles to define the bounds of independent chance. If the unscrambled frequencies fall outside of these bounds, we suggest that there may be evidence that internal climate variability drives correlations between T90 and P10 events, leading to more (or less) frequent extremes.

We also recognize the impact of climate change on T90/P10 compound events and thus analyze results when the forced response is retained. In this case, 1850-1900 is used as the baseline period for percentile calculation and compound events are determined using the same methods as before with the exception that the ensemble mean is not removed.

We then investigate the year of emergence of T90/P10 compound events from internal variability to demonstrate when climate change has or will become a significant influence on the occurrence of T90/P10 compound events under historical and SSP 3-7.0 forcing. As defined here,

compound events emerge from internal variability when the median number of events in the 100-member ensemble exceeds and remains above the 90th percentile of compound events from all members over the 1850-1900 period. Time series of compound events in different locations are visualized by taking a five-year forward moving sum of the events (Figure A.9).

## 2.3 Results and Discussion

### 2.3.1 Role of Internal Variability

We first quantify the influence of internal climate modes on the occurrence of T90/P10 compound events (henceforth referred to as compound events or CEs) by computing frequencies in CESM2-LE from 1850-1950 and ERA5 from 1940-2024. Particular locations, including northern South America, eastern Africa, the Indian subcontinent, and the Indonesian archipelago, depict the highest frequencies of compound events in both the CESM2-LE and ERA5 (Figures 2.1a,b). However, the frequencies in eastern Africa and northern South America encompass more land in ERA5 than in CESM2-LE, expanding into the Congo Rainforest in central Africa and throughout the Amazon Rainforest in northern South America. Frequencies of compound events in the Tibetan Plateau are also higher in ERA5 than they are in CESM2-LE (Figures 2.1a,b).

Internal climate modes influence the dependency between precipitation and temperature anomalies [40] which then impacts the occurrence of compound events [41]. However, even if the temperature and precipitation values are treated as independent variables, random sampling of their distributions would still result in CEs. We use a bootstrapping technique (see Methods) to calculate 99 ensemble-mean frequencies under the null hypothesis of independent, uncorrelated variables. We compare our unscrambled frequencies with the 99 ensemble-mean frequencies under this null hypothesis to analyze where frequencies are greater or less than independent chance. Most of the land areas in the world exhibit frequencies of CEs that are distinguishable from independent chance (Figure 2.1c), and regions with CEs that are not distinguishable from independent chance are often found in transition regions. Dry regions, such as some high-latitude areas and the Saharan

and Arabian deserts, have compound event frequencies that are below independent chance because precipitation and precipitation variance is low.

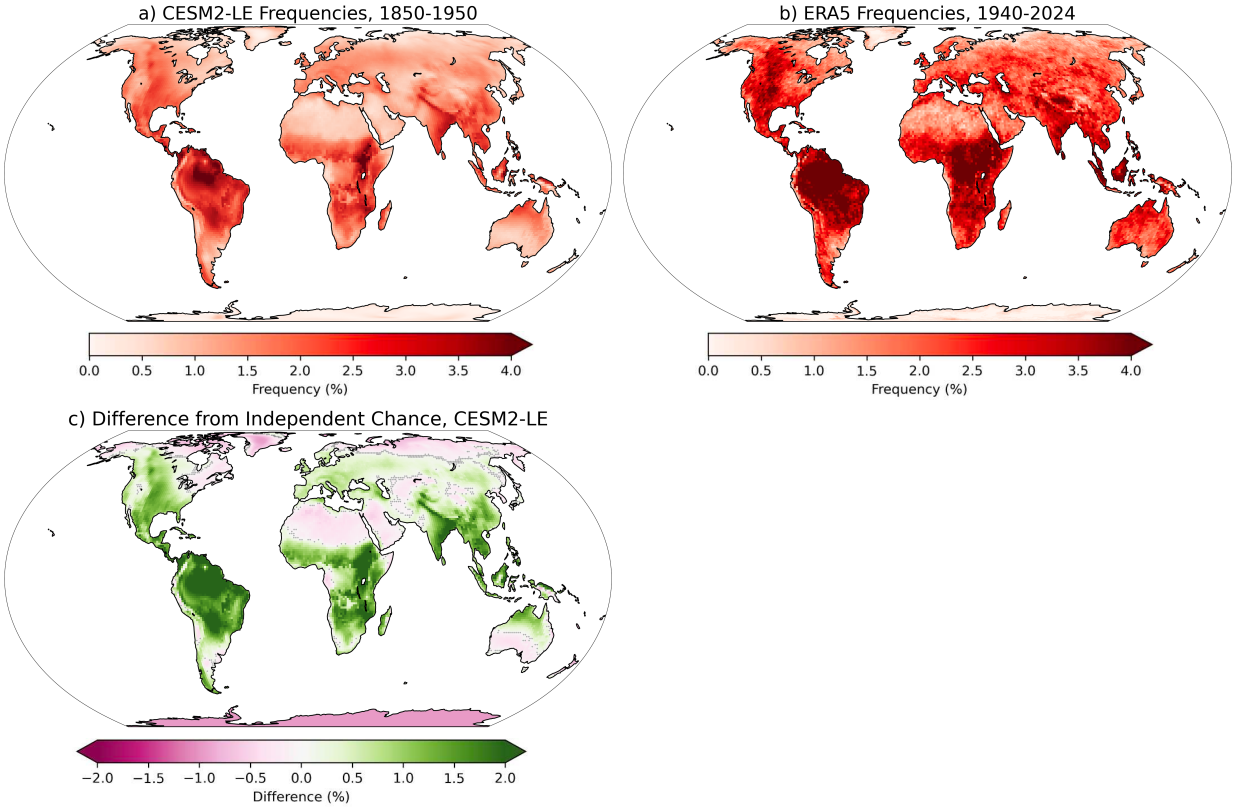


**Figure 2.1:** Frequency of T90/P10 compound events due to detrended anomalies a) 1850-1950 from the 100 member CESM2-LE and b) 1940-2024 ERA5 data. c) Difference of frequencies for CESM2-LE from the average of the 99 scrambled ensemble-mean frequencies under the null hypothesis (see Methods). Stippling indicates where the null hypothesis cannot be rejected and the frequencies of T90/P10 events are consistent with independence. Areas that are shaded green without stippling indicate frequencies of T90/P10 compound events that are greater than independent chance whereas areas that are pink without stippling indicate frequencies that are less than independent chance.

To investigate the connection between internal climate modes and compound events, we first examine the mean sea surface temperature (SST) conditions during months containing compound events at ten different locations (Figures 2.2, A.1, A2). SSTs at specific grid points are selected to build on previous studies investigating internal climate drivers of compound events [9,24,42]. SST patterns in CESM2-LE and ERA5 during compound events over eastern Brazil resemble El Niño (Figures 2.2a, b), the positive phase of the PDO (Figures 2.2a, b), and the positive phase of the IOD

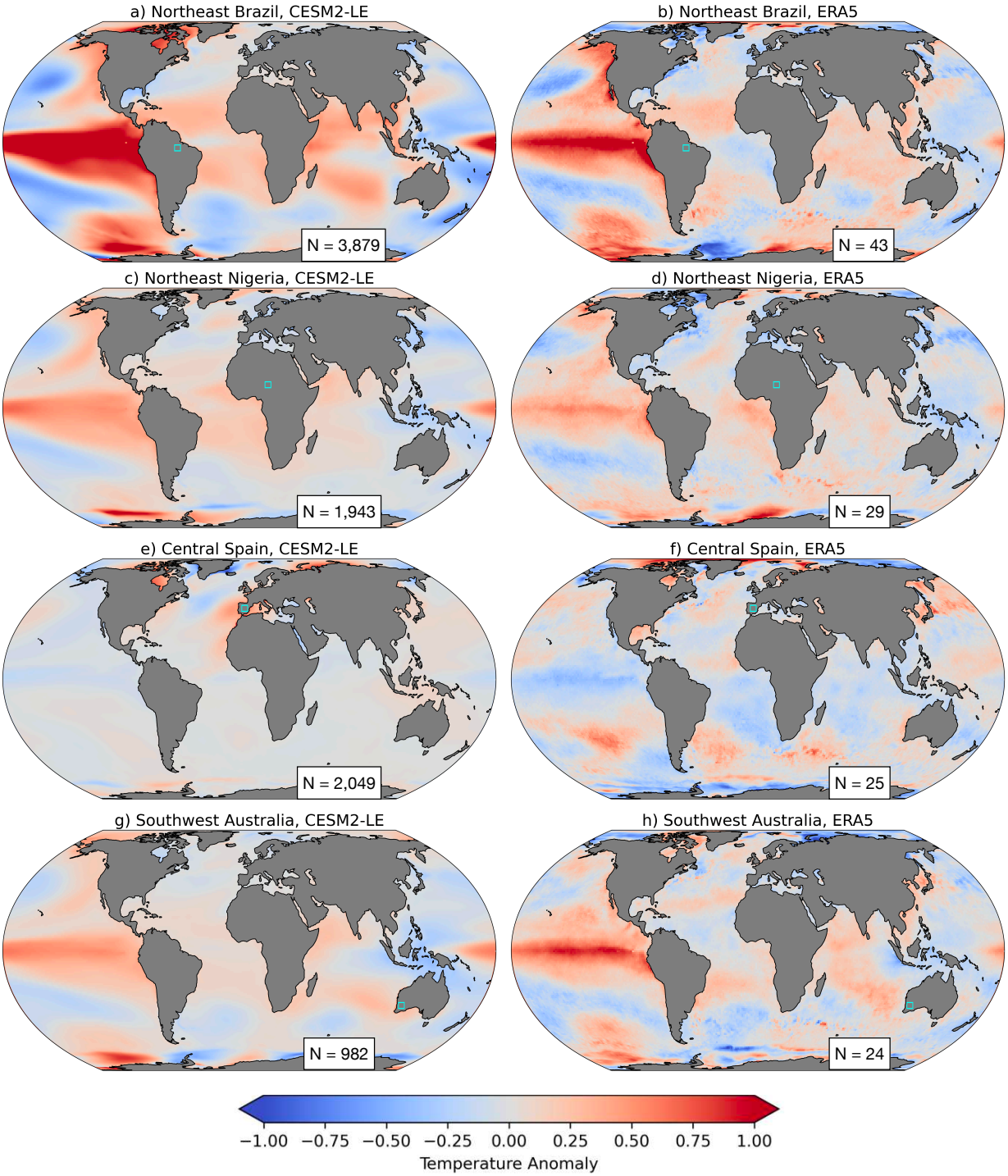


**Figure 2.2:** Mean sea surface temperature (SST) for all months that contain a T90/P10 compound event for a location over (a, b) eastern Brazil (teal box; 3.30 S, 52.50 W), (c, d) Northeast Nigeria (12.72 N, 13.75 E), (e, f) Central Spain (40.05 N, 3.80 W), (g, h) Southwest Australia (30.63 S, 118.80 E). The left column depicts SSTs using 1850-1950 in CESM2-LE and the right column from ERA5, 1940-2024.

(Figures 2.2a, b). SST patterns for northeast Nigeria and southwest Australia exhibit El Niño-like patterns and positive PDO-like patterns (Figures 2.2c,d,g). Thus, we include ENSO, the PDO, and the IOD in the following analysis. Although SST patterns for CEs in central Spain, as well as other locations in Europe, do not strongly resemble SSTs associated with the North Atlantic Oscillation (NAO) (Figures 2.2e, f, A.1, A.2), previous studies [43] have documented the effects of the NAO on temperature and precipitation patterns in Europe and therefore we choose to include this mode in our analysis as well.

The SST patterns that occur during CEs qualitatively indicate how internal climate modes may influence the presence of compound events. We quantify the possible influence of ENSO, PDO, IOD, and the NAO on compound events in CESM2-LE and ERA5 by calculating conditional frequencies of CEs during each phase of each climate mode (Figures 2.3, 2.4). As ENSO is known to drive temperature and precipitation anomalies globally [44, 45], the analysis for PDO, IOD, and the NAO is conditioned on ENSO being in its neutral phase. Conditional frequencies without the neutral ENSO condition are also calculated for comparison and show minor differences except in regions with known strong ENSO teleconnections (Figure A.3). For the calculation of conditional frequencies, we pool all members and sum the number of compound events that occur concurrently with the two phases of the climate modes (e.g. positive PDO and neutral ENSO). We then divide this sum by the total number of months where the two phases of the climate modes are present to determine the conditional frequencies (Figure 2.3). A chi-square test for independence is used to determine if the conditional frequencies are significant relative to our null hypothesis of independent, uncorrelated variables. Grid points where we do not reject the null hypothesis at 98% are represented through the gray shading (Figures 2.3, 2.4). We note that significance is likely much more difficult to obtain using ERA5 due to the low sample size in the reanalysis data (1,008 months) (Figure 2.4). Sample sizes for CESM2-LE are more than 100 times larger than the ERA5 sample sizes, allowing for more confidence in our assessments of where climate modes significantly influence compound events (Figures 2.3, 2.4).

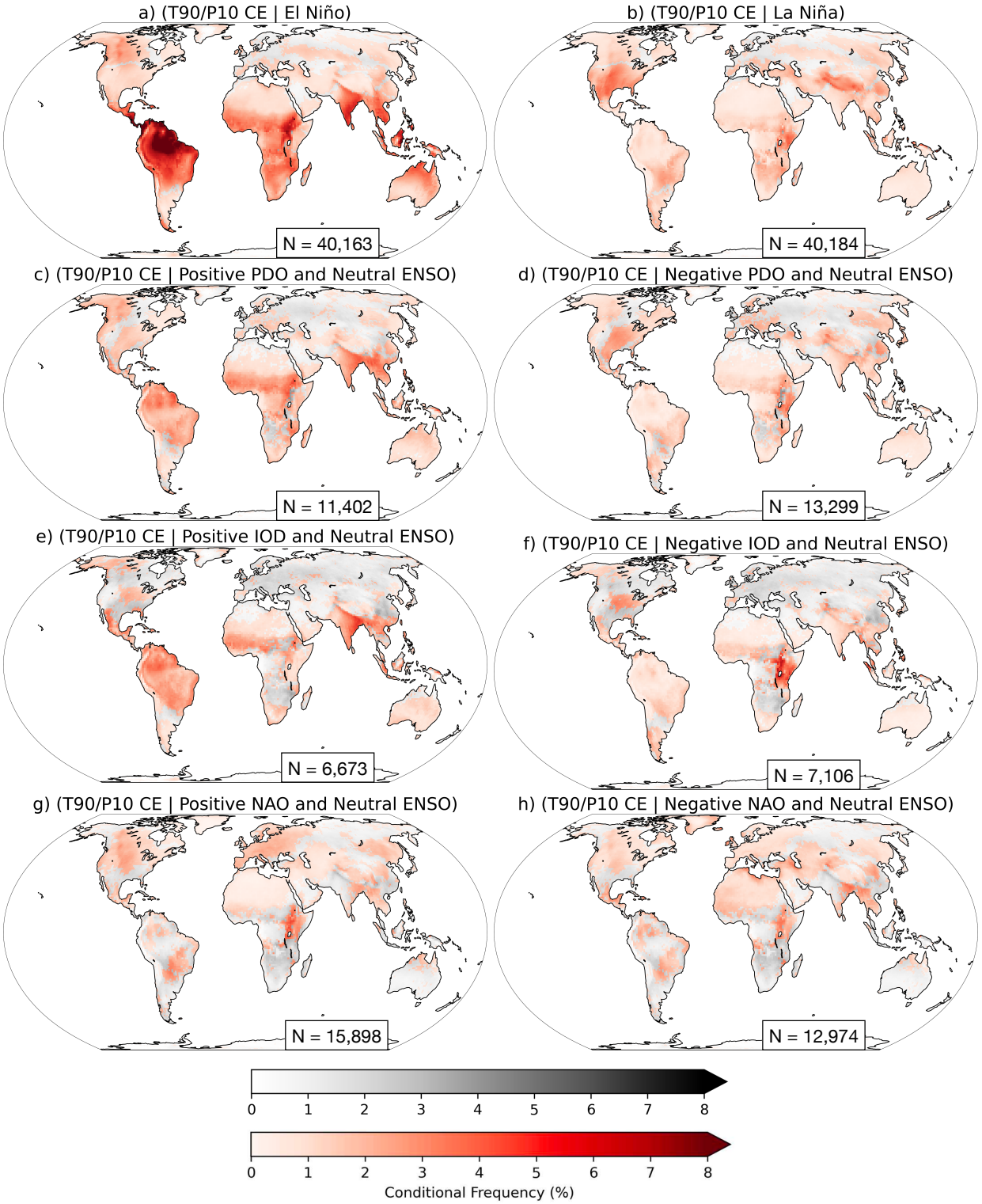


**Figure 2.3:** Conditional frequencies of T90/P10 compound events given a climate mode for detrended anomalies from CESM2-LE (1850-1950). A chi-square test of independence is employed to determine where compound event frequencies can be considered independent of the climate modes and is demonstrated through the gray shading.

For the CESM2-LE, regions with high conditional frequencies during El Niño (Figures 2.3a, 2.4a), such as northern South America, the Indonesian Archipelago, and the Indian subcontinent, can be partially explained by the warmer temperature anomalies and drier conditions that occur during an El Niño month (Figure A.7, A.8). Our ERA5 results for the conditional frequencies for ENSO (Figures 2.4a, b) are consistent with previous studies [42, 46].

Although there are warmer temperature anomalies in Alaska and western Canada during a positive PDO event (Figure A.7), the region does not experience drier precipitation anomalies (Figure A.8). This leads to a low frequency of CEs despite the PDO's influence on temperature (Figure 2.3c). Higher frequencies of CEs in India and southeast Asia during the positive PDO and neutral ENSO phases correspond well with the known precipitation and temperature anomalies associated with the PDO (Figures 2.3c, A.7, A.8). The positive phase of the IOD leads to higher frequencies of compound events in India and the conditional frequencies for the negative phase of the IOD has the highest number of compound events in eastern Africa (Figures 2.3e, f). Figures 2.3g and h depict the NAO's influence on compound events in Europe and lack of influence in the majority of the Southern Hemisphere (Figures 2.3g, h), consistent with known NAO teleconnections [43].

The variability of climate modes may change over the 21st century [47, 48]. With the forced trend still removed, we investigate how the statistics (i.e. conditional frequencies) of CEs change in the future using CESM2-LE and how this may be related, in part, to changes in internal variability. We take the difference in conditional frequencies for the four climate modes between 2000-2100 and 1850-1950 to depict future changes of CE occurrence. A z-test comparison of two proportions is used to determine if our difference in conditional frequencies between the two periods is significant relative to our null hypothesis of equal conditional frequencies.

Future changes in the conditional frequency with El Niño are largest in South America, Africa (south of the Sahara), and the Maritime Continent (Figure 2.5a). As these regions are most impacted by ENSO teleconnections (Figures A.7, A.8) [44], a change in ENSO's amplitude or variability in the CESM2-LE [27, 28] may more strongly impact CEs in these regions compared to other locations. Likewise, the variability and amplitude of the PDO, IOD, and NAO may change

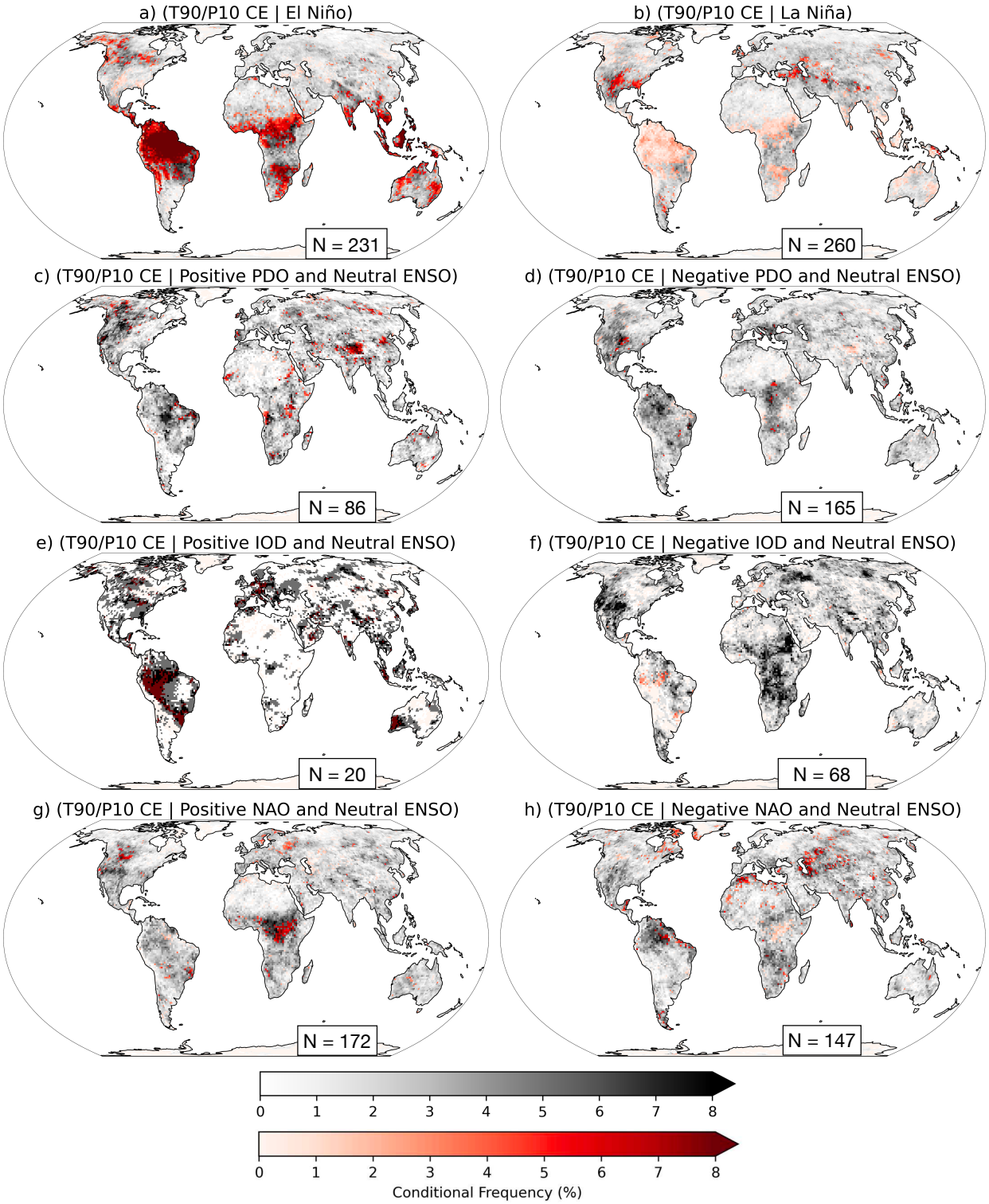


**Figure 2.4:** As in Figure 3, but for ERA5 conditional frequencies from 1940-2024.

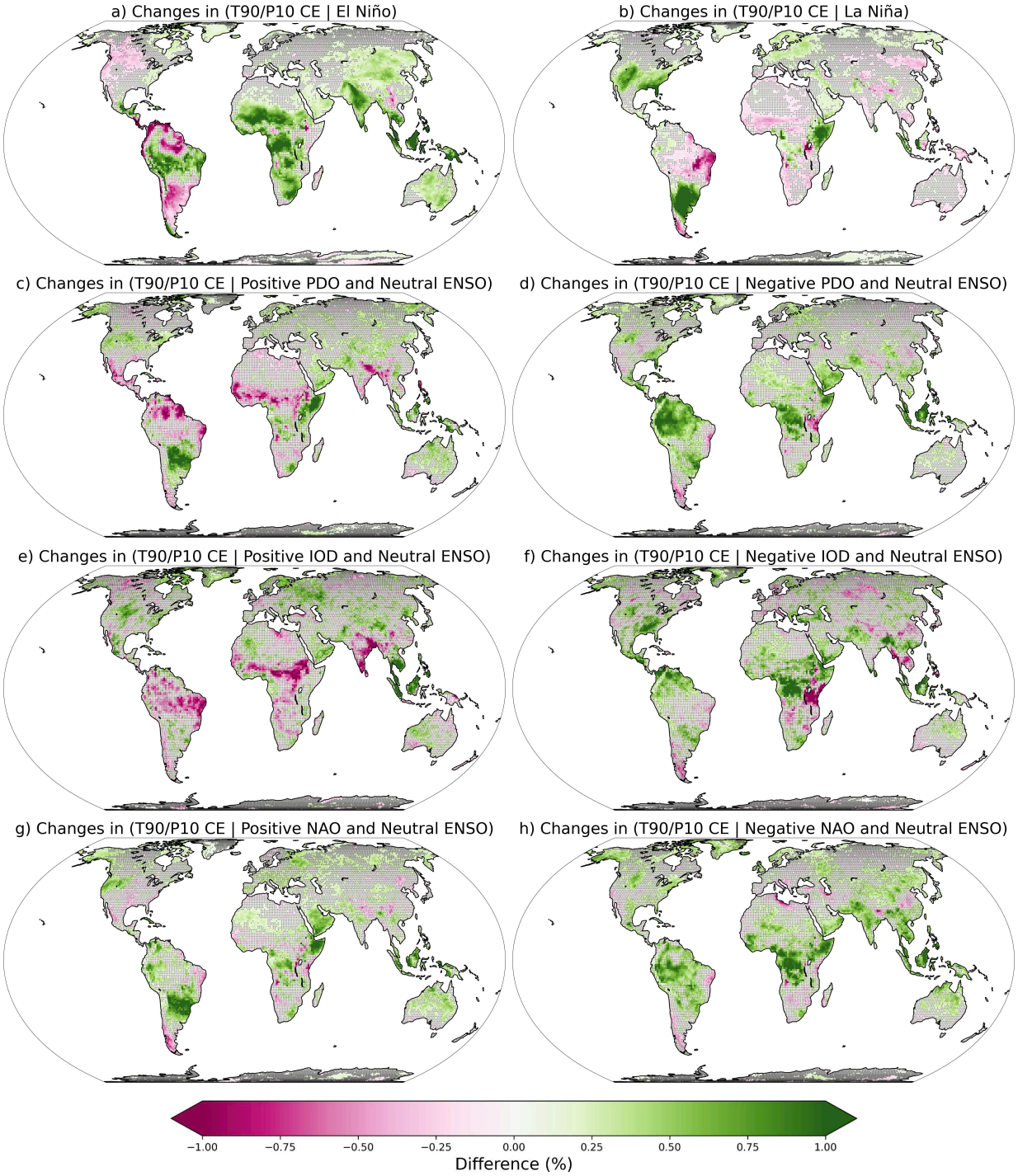


**Figure 2.5:** As in Figure 2.3 but for the changes in conditional frequencies of T90/P10 compound events between 2000-2100 and 1850-1950 in CESM2-LE after removing external forcing. Positive differences in probabilities (green) illustrate that the modes' influence on CEs increases in the future while negative differences in probabilities (pink) illustrate that modes' influence decreases in the future.

throughout the 21st century [49–51]. We find that the conditional frequency changes under the PDO are largest in South America (Figure 2.5c, d), throughout central Africa (Figures 2.5c, d), and in Indonesia in the CESM2-LE (Figure 2.5d). The conditional frequencies under the positive IOD phase increase across the Indonesian archipelago and decrease across the sub-Sahara and India in the future (Figure 2.5e). Although existing literature predicts a decrease in future precipitation over southern Europe under the positive NAO phase [29], the change in conditional frequencies in most of this region does not reject the null hypothesis of equal frequencies (Figure 2.5g). However, under the negative NAO phase we find an increase of compound events over the United Kingdom and Ireland, Iceland, and Scandinavia, while there is a decrease in regions surrounding the Mediterranean (Figure 2.5h). The magnitude of change in conditional frequencies for the NAO is also lower in southern South America when accounting for the PDO's influence (Figures 2.5g, A.6). The changes in conditional frequency between phases for ENSO, PDO, IOD, and the NAO are not identical (or opposite). For example, although conditional frequency for compound events with El Niño increases across Australia in the future, conditional frequencies for La Niña stay approximately the same (Figures 2.5a, b). The future conditional frequencies under the positive IOD phase decrease across the Indian subcontinent but largely stay the same for the negative IOD phase (Figures 2.5e, f).

### 2.3.2 Role of External Forcing

Many studies have documented increasing frequencies of hot and dry compound events under historical and future scenarios [16, 32], but few have examined the time of emergence of CEs from the noise of internal climate variability [34]. Due to the consequential impacts of hot and dry compound events, identifying how they may change over the 21st century is crucial for adaptation planning. We use 1850-1900 as our baseline period, retain the external forcing, and compute the 90th percentile of compound events of the 100 members in CESM2-LE at all grid points. The year of emergence from internal variability is defined to be when the median number of CEs in a five-

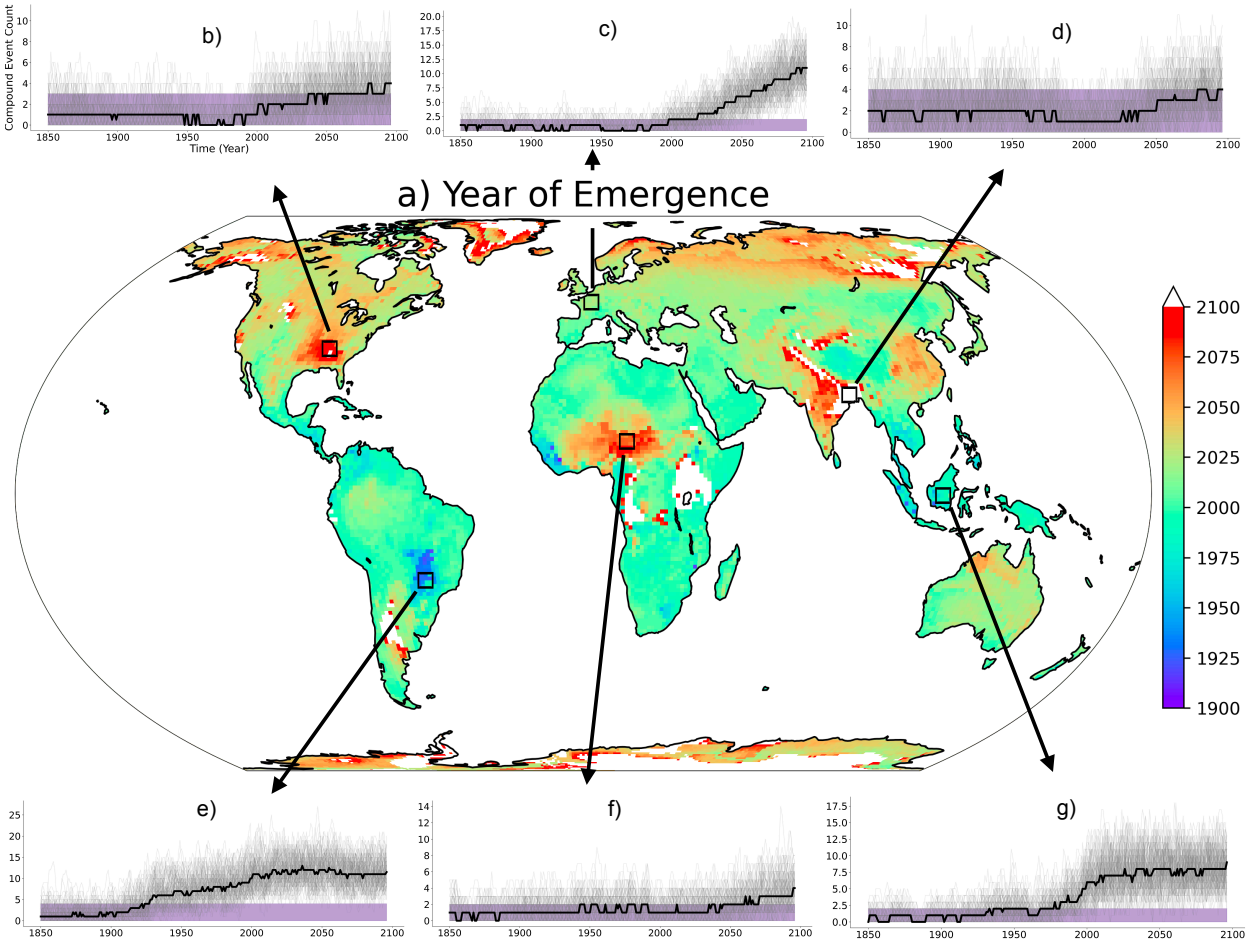


**Figure 2.6:** a) Year of emergence for the ensemble median. White indicates no emergence from the 90th percentile before 2096. Time series of the five-year forward moving sum of compound events shown for six locations: b) southeast United States (35.34 N, 88.80 W), c) northern France (48.53 N, 2.50 W), d) northeast India (24.03 N, 87.50 E), e) southeast Brazil (20.26 S, 51.20 W), f) northeast Nigeria (12.72 N, 13.75 E), g) eastern Indonesia (0.47 S, 113.80 E).

year forward moving sum at every grid point exceeds the 90th percentile of the baseline (Figure A.9).

We find that compound events emerge from internal variability before 2025 for most land regions under SSP 3-7.0 (60% of land area, excluding Antartica, Figure 2.6a). The majority of the Southern Hemisphere emerges prior to 2025 (87% of land area, excluding Antartica), except for portions of central Africa and southern South America. In contrast, there is far more heterogeneity in emergence timing over the Northern Hemisphere, with only 50% of the land area emerging prior to 2025 (Figure 2.6c). Regions with the highest frequency of CEs in the early historical period

(Figure 2.1a, c) display a wide range of emergence times. For example, northern Brazil and eastern Africa exhibit similar frequencies of CEs between 1850-1950 (Figure 2.1a), but northern Brazil emerges around 2003 while eastern Africa still has not emerged by the end of the 21st century (Figure 2.6a). Differences in precipitation trends could account for the emergence differences as there is a decrease in precipitation over northern Brazil in the 21st century and an increase in precipitation over eastern Africa, including South Sudan and Uganda (Figure A.12). Southern Brazil and western Africa exhibit relatively early emergence times (prior to 1965), which may be driven, at least in part, by the decrease in natural vegetation during that time (Figure A.10).

Time series of compound events for fourteen locations are shown in Figures 2.6b-g and A.11. Over northern France, as well as other locations across Europe, a consistently increasing trend of compound events is evident early in the 21st century (Figure 2.6c, A.11). This result is consistent with projections of the global average of hot and dry compound events under SSP 3-7.0 found in previous studies [13, 17]. However, for locations exhibiting earlier emergence, including southern Brazil and the Indonesian Archipelago, emergence during the 20th century is followed by stabilization of CE frequencies. This could be due to observed decrease in natural vegetation in the mid-twentieth century combined with unchanged precipitation patterns across the 21st century compared to the historical period (Figures 2.6e, g, A.10, A.13). Other regions with historically low frequencies, including northeast India and northeast Nigeria, show minimal changes under climate change (Figures 2.6d, f).

## 2.4 Conclusion

In this study, we explored the roles of internal climate variability and external forcing as drivers for hot and dry compound events in the CESM2-LE, defined by using the 90th percentile of monthly temperature and the 10th percentile of monthly precipitation rate at each land gridpoint over the globe. We analyzed the influence of the El Niño Southern Oscillation (ENSO), the Pacific Decadal Oscillation (PDO), the Indian Ocean Dipole (IOD), and the North Atlantic Oscillation (NAO) on compound events through calculations of conditional frequencies. We found that ENSO

had the largest impact on northern South America, the Indonesian archipelago, and the Indian subcontinent (Figure 2.3a, b) and that conditional frequencies for the positive PDO are higher in southeast Asia than in Alaska and western Canada, most likely due to precipitation anomaly differences that occur during the positive PDO phase across these regions (Figures 2.3c, d, A.8). The IOD has the most influence over eastern Africa and the Indian subcontinent (Figures 2.3e, f). The NAO impacts the conditional frequencies of CEs over Europe (Figures 2.3g, h).

Although previous comparisons have been made for the changing magnitude, occurrence, and severity of compound events due to future increases in external forcing [13, 14, 17, 32], we add to this by exploring when the occurrence of compound events emerges from internal variability under SSP 3-7.0 (Figure 2.6a). We find that under climate change, the frequency of compound events emerges from the noise of internal variability over many land areas before 2025. Regions with compound events that emerged before 1975, such as southeastern Brazil, may have emerged earlier due to changes in natural vegetation (Figure A.10). We also find differences in the regional timeseries of these events (Figures 2.6b-g), and not all locations (i.e. southeast United States, northeast India) coincide with the average global projection of compound events under SSP 3-7.0 [17]. This could be, in part, due to the influence of internal climate variability (Figures 2.4, A.3) as well as precipitation pattern changes (Figures A.12-15).

Our results demonstrate the utility of the CESM2-LE to advance understanding of large-scale, unforced, internal climate variability and external forcing as drivers of hot and dry compound events. Although external forcing will impact compound events in the future over many regions, we show that internal variability will continue to be a strong influence. To quantify this influence, we first used SST composite maps during compound event months to motivate our choice of climate modes. We then leveraged the CESM2-LE to provide a comprehensive global analysis of four large-scale climate modes. Our analysis of the joint influence of ENSO, PDO, IOD, and NAO as drivers of hot and dry CEs adds to the literature that has almost exclusively focused on ENSO's influence. We then quantified frequency differences between the historical and future period due to possible changes in future internal variability.

The time of emergence of compound events is underexplored. We quantified the time of emergence of hot and dry CEs under SSP 3-7.0 and visualized the spatiotemporal patterns associated with this emergence. Investigation into other scenarios would assist in understanding the range of possible CE emergence. Expanding such analyses can improve understanding of these events' response to internal and external climate drivers, aiding in preparation for the future compound event changes.

# Chapter 3

# Future Work

In this thesis, we first investigated internal variability as a driver of hot and dry compound events in CESM2-LE. This work could be expanded to explore combinations of the four mode phases in our study – ENSO, PDO, IOD, and NAO – and how their interactions influence the frequency of hot and dry compound events. Understanding how combinations of drivers dampen or amplify the occurrence of compound events would enhance regional preparation capabilities. Leveraging a large ensemble to examine combinations of modes at a global scale allows a larger sample size of co-occurring modes than if observations alone were used, which has been demonstrated in regional-scale analysis [25]. Incorporating this on a global scale provides information on drivers of compound events for regions, such as the "Global South", where such studies are lacking [18]. Furthermore, the incorporation of other large-scale modes that have been shown to exert influence over hot and dry compound events in specific regions, such as the Atlantic Multidecadal Oscillation (AMO) [8], could also be included in future studies.

In this work, we also found that under SSP 3-7.0, which is a particularly high emission scenario, 60% of land area (excluding Antarctica) emerged before 2025. Exploring the emergence of compound event frequency in higher and lower emission scenarios (i.e. SSP 5-8.5, SSP 2-4.5) would further assist in understanding the potential range of compound event occurrence in the 21st century. Furthermore, regions may temporarily emerge from internal variability and then return to the range of internal variability before ultimately emerging or not emerging by the end of the century. This concept can be referred to as the period of emergence and drivers of this temporary emergence may vary across different regions [34]. Further study on the period of emergence including what drives them would assist in sectors such as agriculture due to enhanced prediction capabilities. For example, while a region in eastern Africa does not emerge by the end of the 21st century in our study (Figure 6a), certain locations within the region experienced increased compound events above the range of internal variability for multiple decades before returning. This

could lead to heightened impacts during this period of emergence compared to when the compound event occurrence is within the range of internal variability.

Hot and wet compound events, pertaining to either flooding and extreme heat or humid heat/heat stress, can also lead to human health impacts [23]. Evaluation of these extremes is not analyzed as often as hot and dry extremes [18, 52]. Existing literature has shown changing occurrences of hot and wet compound events both in historical analysis [53] and in future scenarios [16, 32, 54], and are attributed to climate change [55]. Knowledge of the time of emergence as well as the period(s) of emergence for these events is lacking and should be investigated to further understand how these compound events respond to climate change. This could be done using SSP 3-7.0 in CESM2-LE as well as other emission scenarios. Exploring the role of internal variability as drivers of hot and wet compound events could then be investigated through use of the large ensemble to assist in explaining the time and period(s) of emergence of hot and wet events.

# Bibliography


[1] Raymond P Motha. The impact of extreme weather events on agriculture in the united states. In *Challenges and Opportunities in Agrometeorology*, pages 397–407. Springer Berlin Heidelberg, Berlin, Heidelberg, 2011.

[2] G Greenough, M McGeehin, S M Bernard, J Trtanj, J Riad, and D Engelberg. The potential impacts of climate variability and change on health impacts of extreme weather events in the united states. *Environ. Health Perspect.*, 109 Suppl 2(suppl 2):191–198, May 2001.

[3] Kenneth E Kunkel, Roger A Pielke, Jr, and Stanley A Changnon. Temporal fluctuations in weather and climate extremes that cause economic and human health impacts: A review. *Bull. Am. Meteorol. Soc.*, 80(6):1077–1098, June 1999.

[4] S E Perkins and E M Fischer. The usefulness of different realizations for the model evaluation of regional trends in heat waves. *Geophys. Res. Lett.*, 40(21):5793–5797, November 2013.

[5] A M Vicedo-Cabrera, N Scovronick, F Sera, D Royé, R Schneider, A Tobias, C Astrom, Y Guo, Y Honda, D M Hondula, R Abrutzky, S Tong, M de Sousa Zanotti Stagliorio Coelho, P H Nascimento Saldiva, E Lavigne, P Matus Correa, N Valdes Ortega, H Kan, S Osorio, J Kyselý, A Urban, H Orru, E Indermitte, J J K Jaakkola, N Ryti, M Pascal, A Schneider, K Katsouyanni, E Samoli, F Mayvaneh, A Entezari, P Goodman, A Zeka, P Michelozzi, F de'Donato, M Hashizume, B Alahmad, M Hurtado Diaz, C De La Cruz Valencia, A Overcenco, D Houthuijs, C Ameling, S Rao, F Di Ruscio, G Carrasco-Escobar, X Seposo, S Silva, J Madureira, I H Holobaca, S Fratianni, F Acquaotta, H Kim, W Lee, C Iniguez, B Forsberg, M S Ragettli, Y L L Guo, B Y Chen, S Li, B Armstrong, A Aleman, A Zanobetti, J Schwartz, T N Dang, D V Dung, N Gillett, A Haines, M Mengel, V Huber, and A Gasparrini. The burden of heat-related mortality attributable to recent human-induced climate change. *Nat. Clim. Chang.*, 11(6):492–500, June 2021.

[6] S E Perkins-Kirkpatrick and S C Lewis. Increasing trends in regional heatwaves. *Nat. Commun.*, 11(1):3357, July 2020.

[7] Emanuele Bevacqua, Laura Suarez-Gutierrez, Aglaé Jézéquel, Flavio Lehner, Mathieu Vrac, Pascal Yiou, and Jakob Zscheischler. Advancing research on compound weather and climate events via large ensemble model simulations. *Nat. Commun.*, 14(1):2145, April 2023.

[8] Xinying Wu, Zengchao Hao, Fanghua Hao, Xuan Zhang, Vijay P Singh, and Cheng Sun. Influence of large-scale circulation patterns on compound dry and hot events in china. *J. Geophys. Res.*, 126(4), February 2021.

[9] Zengchao Hao, Fanghua Hao, Vijay P Singh, and Xuan Zhang. Quantifying the relationship between compound dry and hot events and el niño–southern oscillation (ENSO) at the global scale. *J. Hydrol.*, 567:332–338, December 2018.

[10] Timo Kelder, Dorothy Heinrich, Lisette Klok, Vikki Thompson, Henrique M D Goulart, Ed Hawkins, Louise J Slater, Laura Suarez-Gutierrez, Robert L Wilby, Erin Coughlan de Perez, Elisabeth M Stephens, Stephen Burt, Bart van den Hurk, Hylke de Vries, Karin van der Wiel, E Lisa F Schipper, Antonio Carmona Baéz, Ellen van Bueren, and Erich M Fischer. How to stop being surprised by unprecedented weather. *Nat. Commun.*, 16(1):2382, March 2025.

[11] Jakob Zscheischler, Olivia Martius, Seth Westra, Emanuele Bevacqua, Colin Raymond, Radley M Horton, Bart van den Hurk, Amir AghaKouchak, Aglaé Jézéquel, Miguel D Mahecha, Douglas Maraun, Alexandre M Ramos, Nina N Ridder, Wim Thiery, and Edoardo Vignotto. A typology of compound weather and climate events. *Nature Reviews Earth & Environment*, 1(7):333–347, June 2020.

[12] IPCC. *Managing the Risks of Extreme Events and Disasters to Advance Climate Change Adaptation*. Cambridge University Press, Cambridge, UK, 2012.

[13] Johannes Vogel, Eva Paton, Valentin Aich, and Axel Bronstert. Increasing compound warm spells and droughts in the mediterranean basin. *Weather and Climate Extremes*, 32:100312, June 2021.

[14] Sourav Mukherjee and Ashok Kumar Mishra. Increase in compound drought and heatwaves in a warming world. *Geophys. Res. Lett.*, 48(1), January 2021.

[15] Kumar P Tripathy, Sourav Mukherjee, Ashok K Mishra, Michael E Mann, and A Park Williams. Climate change will accelerate the high-end risk of compound drought and heatwave events. *Proc. Natl. Acad. Sci. U. S. A.*, 120(28):e2219825120, July 2023.

[16] Yu Meng, Zengchao Hao, Sifang Feng, Xuan Zhang, and Fanghua Hao. Increase in compound dry-warm and wet-warm events under global warming in CMIP6 models. *Glob. Planet. Change*, 210:103773, March 2022.

[17] Qin Zhang, Dunxian She, Liping Zhang, Gangsheng Wang, Jie Chen, and Zengchao Hao. High sensitivity of compound drought and heatwave events to global warming in the future. *Earths Future*, 10(11), November 2022.

[18] Lou Brett, Christopher J White, Daniela I V Domeisen, Bart van den Hurk, Philip Ward, and Jakob Zscheischler. Review article: The growth in compound weather events research in the decade since SREX. September 2024.

[19] K. B. Rodgers, S.-S. Lee, N. Rosenbloom, A. Timmermann, G. Danabasoglu, C. Deser, J. Edwards, J.-E. Kim, I. R. Simpson, K. Stein, M. F. Stuecker, R. Yamaguchi, T. Bódai, E.-S. Chung, L. Huang, W. M. Kim, J.-F. Lamarque, D. L. Lombardozzi, W. R. Wieder, and S. G. Yeager. Ubiquity of human-induced changes in climate variability. *Earth System Dynamics*, 12(4):1393–1411, 2021.

[20] G Danabasoglu, J-F Lamarque, J Bacmeister, D A Bailey, A K DuVivier, J Edwards, L K Emmons, J Fasullo, R Garcia, A Gettelman, C Hannay, M M Holland, W G Large, P H Lauritzen, D M Lawrence, J T M Lenaerts, K Lindsay, W H Lipscomb, M J Mills, R Neale, K W

Oleson, B Otto-Bliesner, A S Phillips, W Sacks, S Tilmes, L Kampenhout, M Vertenstein, A Bertini, J Dennis, C Deser, C Fischer, B Fox-Kemper, J E Kay, D Kinnison, P J Kushner, V E Larson, M C Long, S Mickelson, J K Moore, E Nienhouse, L Polvani, P J Rasch, and W G Strand. The community earth system model version 2 (CESM2). *J. Adv. Model. Earth Syst.*, 12(2), February 2020.

[21] Hossein Tabari and Patrick Willems. Global risk assessment of compound hot-dry events in the context of future climate change and socioeconomic factors. *npj Climate and Atmospheric Science*, 6(1):1–10, June 2023.

[22] Laura Niggli, Christian Huggel, Veruska Muccione, Raphael Neukom, and Nadine Salzmann. Towards improved understanding of cascading and interconnected risks from concurrent weather extremes: Analysis of historical heat and drought extreme events. *PLOS Clim*, 1(8):e0000057, August 2022.

[23] Jakob Zscheischler, Bart van den Hurk, Philip J Ward, and Seth Westra. Chapter 4 - multivariate extremes and compound events. In Jana Sillmann, Sebastian Sippel, and Simone Russo, editors, *Climate Extremes and Their Implications for Impact and Risk Assessment*, pages 59–76. Elsevier, jan 2020.

[24] Sourav Mukherjee, Moetasim Ashfaq, and Ashok Kumar Mishra. Compound drought and heatwaves at a global scale: The role of natural climate variability-associated synoptic patterns and land-surface energy budget anomalies. *J. Geophys. Res.*, 125(11), June 2020.

[25] P Jyoteeshkumar Reddy, Sarah E Perkins-Kirkpatrick, Nina N Ridder, and Jason J Sharples. Combined role of ENSO and IOD on compound drought and heatwaves in australia using two CMIP6 large ensembles. *Weather and Climate Extremes*, 37:100469, September 2022.

[26] Youichi Kamae, Hideo Shiogama, Yukiko Imada, Masato Mori, Osamu Arakawa, Ryo Mizuta, Kohei Yoshida, Chiharu Takahashi, Miki Arai, Masayoshi Ishii, Masahiro Watanabe, Masahide Kimoto, Shang-Ping Xie, and Hiroaki Ueda. Forced response and internal

variability of summer climate over western north america. *Clim. Dyn.*, 49(1):403–417, July 2017.

[27] Nicola Maher, Robert C Jnglin Wills, Pedro DiNezio, Jeremy Klavans, Sebastian Milinski, Sara C Sanchez, Samantha Stevenson, Malte F Stuecker, and Xian Wu. The future of the el Niño–Southern oscillation: using large ensembles to illuminate time-varying responses and inter-model differences. *Earth Syst. Dyn.*, 14(2):413–431, April 2023.

[28] Wenju Cai, Benjamin Ng, Guojian Wang, Agus Santoso, Lixin Wu, and Kai Yang. Increased ENSO sea surface temperature variability under four IPCC emission scenarios. *Nat. Clim. Chang.*, 12(3):228–231, March 2022.

[29] C M McKenna and A C Maycock. The role of the north atlantic oscillation for projections of winter mean precipitation in europe. *Geophys. Res. Lett.*, 49(19), October 2022.

[30] Wenju Cai, Guojian Wang, Agus Santoso, Michael J McPhaden, Lixin Wu, Fei-Fei Jin, Axel Timmermann, Mat Collins, Gabriel Vecchi, Matthieu Lengaigne, Matthew H England, Dietmar Dommenget, Ken Takahashi, and Eric Guilyardi. Increased frequency of extreme la niña events under greenhouse warming. *Nat. Clim. Chang.*, 5(2):132–137, February 2015.

[31] Clara Deser, Adam S Phillips, Michael A Alexander, Dillon J Amaya, Antonietta Capotondi, Michael G Jacox, and James D Scott. Future changes in the intensity and duration of marine heat and cold waves: Insights from coupled model initial-condition large ensembles. *J. Clim.*, 37(6):1877–1902, March 2024.

[32] Yi Wu, Chiyuan Miao, Ying Sun, Amir AghaKouchak, Chenwei Shen, and Xuewei Fan. Global observations and CMIP6 simulations of compound extremes of monthly temperature and precipitation. *GeoHealth*, 5(5):e2021GH000390, May 2021.

[33] Hans Hersbach, Bill Bell, Paul Berrisford, Shoji Hirahara, András Horányi, Joaquín Muñoz-Sabater, Julien Nicolas, Carole Peubey, Raluca Radu, Dinand Schepers, Adrian Simmons,

Cornel Soci, Saleh Abdalla, Xavier Abellan, Gianpaolo Balsamo, Peter Bechtold, Gionata Biavati, Jean Bidlot, Massimo Bonavita, Giovanna De Chiara, Per Dahlgren, Dick Dee, Michail Diamantakis, Rossana Dragani, Johannes Flemming, Richard Forbes, Manuel Fuentes, Alan Geer, Leo Haimberger, Sean Healy, Robin J Hogan, Elías Hólm, Marta Janisková, Sarah Keeley, Patrick Laloyaux, Philippe Lopez, Cristina Lupu, Gabor Radnoti, Patricia de Rosnay, Iryna Rozum, Freja Vamborg, Sebastien Villaume, and Jean-Noël Thépaut. The ERA5 global reanalysis. *Q. J. R. Meteorol. Soc.*, 146(730):1999–2049, July 2020.

[34] Joséphine Schmutz, Mathieu Vrac, Bastien François, and Burak Bulut. Spatial structures of emerging hot & dry compound events over europe from 1950 to 2023. February 2025.

[35] V. Eyring, S. Bony, G. A. Meehl, C. A. Senior, B. Stevens, R. J. Stouffer, and K. E. Taylor. Overview of the coupled model intercomparison project phase 6 (cmip6) experimental design and organization. *Geoscientific Model Development*, 9(5):1937–1958, 2016.

[36] N. Maher, A. S. Phillips, C. Deser, R. C. J. Wills, F. Lehner, J. Fasullo, J. M. Caron, L. Brunner, and U. Beyerle. The updated multi-model large ensemble archive and the climate variability diagnostics package: New tools for the study of climate variability and change. *EGUsphere*, 2024:1–28, 2024.

[37] Adam S Phillips, Clara Deser, and John Fasullo. Evaluating modes of variability in climate models. *Eos (Washington DC)*, 95(49):453–455, December 2014.

[38] James W Hurrell and Clara Deser. North atlantic climate variability: The role of the north atlantic oscillation. *J. Mar. Syst.*, 78(1):28–41, August 2009.

[39] Uwe Schulzweida. Cdo user guide, October 2023.

[40] Sifang Feng and Zengchao Hao. Quantitative contribution of ENSO to precipitation-temperature dependence and associated compound dry and hot events. *Atmos. Res.*, 260:105695, October 2021.

[41] Jakob Zscheischler and Sonia I Seneviratne. Dependence of drivers affects risks associated with compound events. *Sci Adv*, 3(6):e1700263, June 2017.

[42] Zengchao Hao, Xuan Zhang, Vijay P Singh, and Fanghua Hao. Joint modeling of precipitation and temperature under influences of el niño southern oscillation for compound event evaluation and prediction. *Atmos. Res.*, 245:105090, November 2020.

[43] James W Hurrell and Harry Van Loon. DECADAL VARIATIONS IN CLIMATE ASSOCIATED WITH THE NORTH ATLANTIC OSCILLATION. *Clim. Change*, 36(3/4):301–326, 1997.

[44] Nathan J L Lenssen, Lisa Goddard, and Simon Mason. Seasonal forecast skill of ENSO teleconnection maps. *Weather Forecast.*, 35(6):2387–2406, December 2020.

[45] M Latif and N S Keenlyside. El niño/southern oscillation response to global warming. *Proc. Natl. Acad. Sci. U. S. A.*, 106(49):20578–20583, December 2009.

[46] Yu Zhang, Zengchao Hao, Sifang Feng, Xuan Zhang, and Fanghua Hao. Changed relationship between compound dry-hot events and ENSO at the global scale. *J. Hydrol.*, 621:129559, June 2023.

[47] Wenju Cai, Agus Santoso, Matthew Collins, Boris Dewitte, Christina Karamperidou, Jong-Seong Kug, Matthieu Lengaigne, Michael J McPhaden, Malte F Stuecker, Andréa S Taschetto, Axel Timmermann, Lixin Wu, Sang-Wook Yeh, Guojian Wang, Benjamin Ng, Fan Jia, Yun Yang, Jun Ying, Xiao-Tong Zheng, Tobias Bayr, Josephine R Brown, Antonietta Capotondi, Kim M Cobb, Bolan Gan, Tao Geng, Yoo-Geun Ham, Fei-Fei Jin, Hyun-Su Jo, Xichen Li, Xiaopei Lin, Shayne McGregor, Jae-Heung Park, Karl Stein, Kai Yang, Li Zhang, and Wenxiu Zhong. Changing el Niño–Southern oscillation in a warming climate. *Nat. Rev. Earth Environ.*, 2(9):628–644, August 2021.

[48] Tao Geng, Yun Yang, and Lixin Wu. On the mechanisms of pacific decadal oscillation modulation in a warming climate. *J. Clim.*, 32(5):1443–1459, March 2019.

[49] Abolfazl Rezaei, Khalil Karami, Simone Tilmes, and John C Moore. Changes in global teleconnection patterns under global warming and stratospheric aerosol intervention scenarios. *Atmos. Chem. Phys.*, 23(10):5835–5850, May 2023.

[50] Clara Deser, James W Hurrell, and Adam S Phillips. The role of the north atlantic oscillation in european climate projections. *Clim. Dyn.*, 49(9-10):3141–3157, November 2017.

[51] Wenju Cai, Simon Borlace, Matthieu Lengaigne, Peter van Rensch, Mat Collins, Gabriel Vecchi, Axel Timmermann, Agus Santoso, Michael J McPhaden, Lixin Wu, Matthew H England, Guojian Wang, Eric Guilyardi, and Fei-Fei Jin. Increasing frequency of extreme el niño events due to greenhouse warming. *Nat. Clim. Chang.*, 4(2):111–116, February 2014.

[52] Wei Zhang, Ming Luo, Si Gao, Weilin Chen, Vittal Hari, and Abdou Khouakhi. Compound hydrometeorological extremes: Drivers, mechanisms and methods. *Front. Earth Sci.*, 9, October 2021.

[53] Kelsey E Ennis and Shawn M Milrad. Man, it's a hot one: Trends and extremes in florida autumn heat stress. *Int. J. Climatol.*, March 2024.

[54] Martha M Vogel, Mathias Hauser, and Sonia I Seneviratne. Projected changes in hot, dry and wet extreme events' clusters in CMIP6 multi-model ensemble. *Environ. Res. Lett.*, 15(9):094021, August 2020.

[55] Jianxin Zeng, Shulei Zhang, Sha Zhou, Xingjie Lu, Omarjan Obulkasim, Han Zhang, and Yongjiu Dai. Comparison of the risks and drivers of compound hot-dry and hot-wet extremes in a warming world. *Environ. Res. Lett.*, September 2024.

# Appendix A

# Supplementary Figures

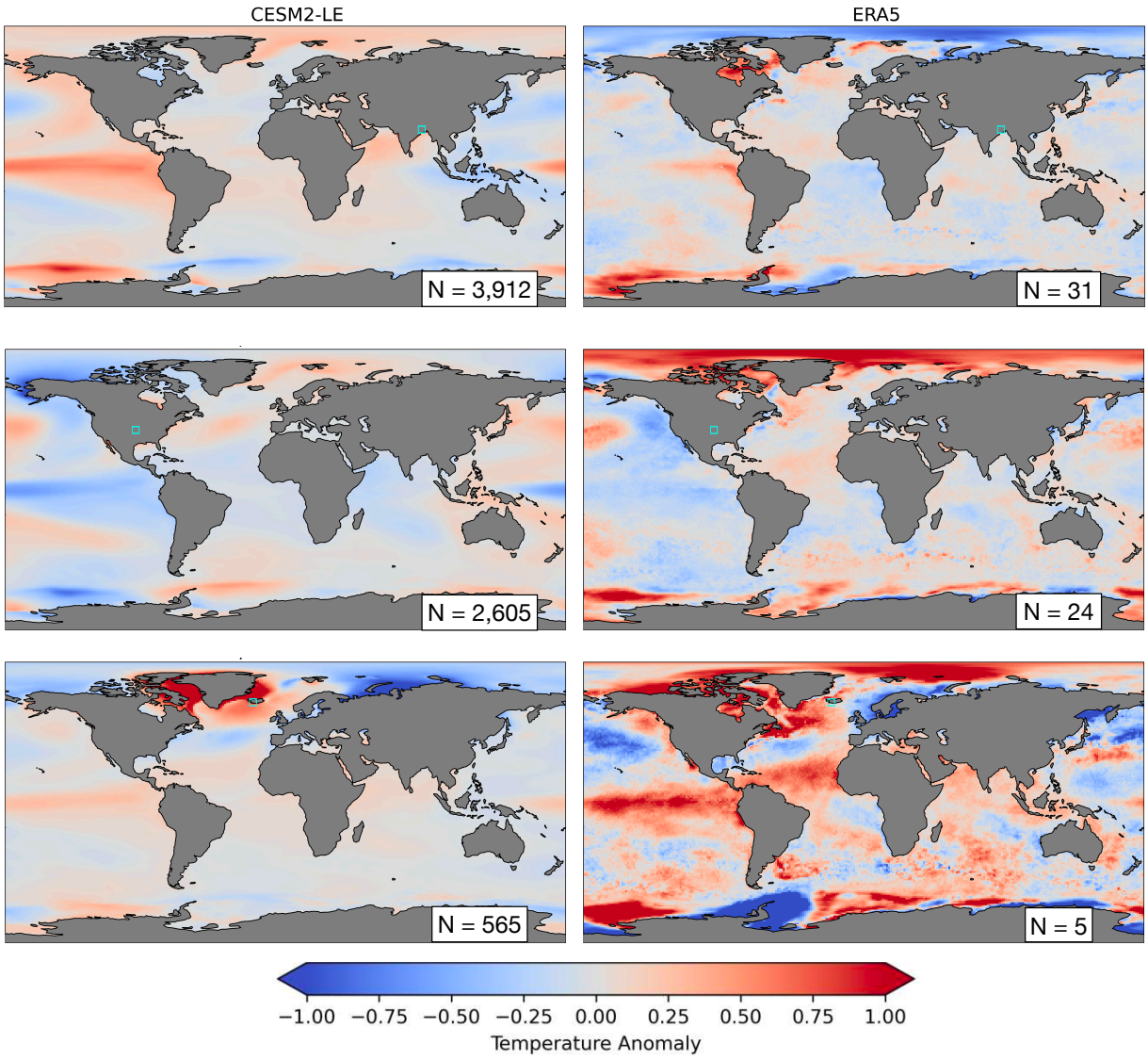


**Figure A.1:** As in Figure 2 but for northeast India (24.03 N, 87.5 E), central United States (38.17 N, 96.2 W), and Reykjavik, Iceland (64.55 N, 22.2 W).

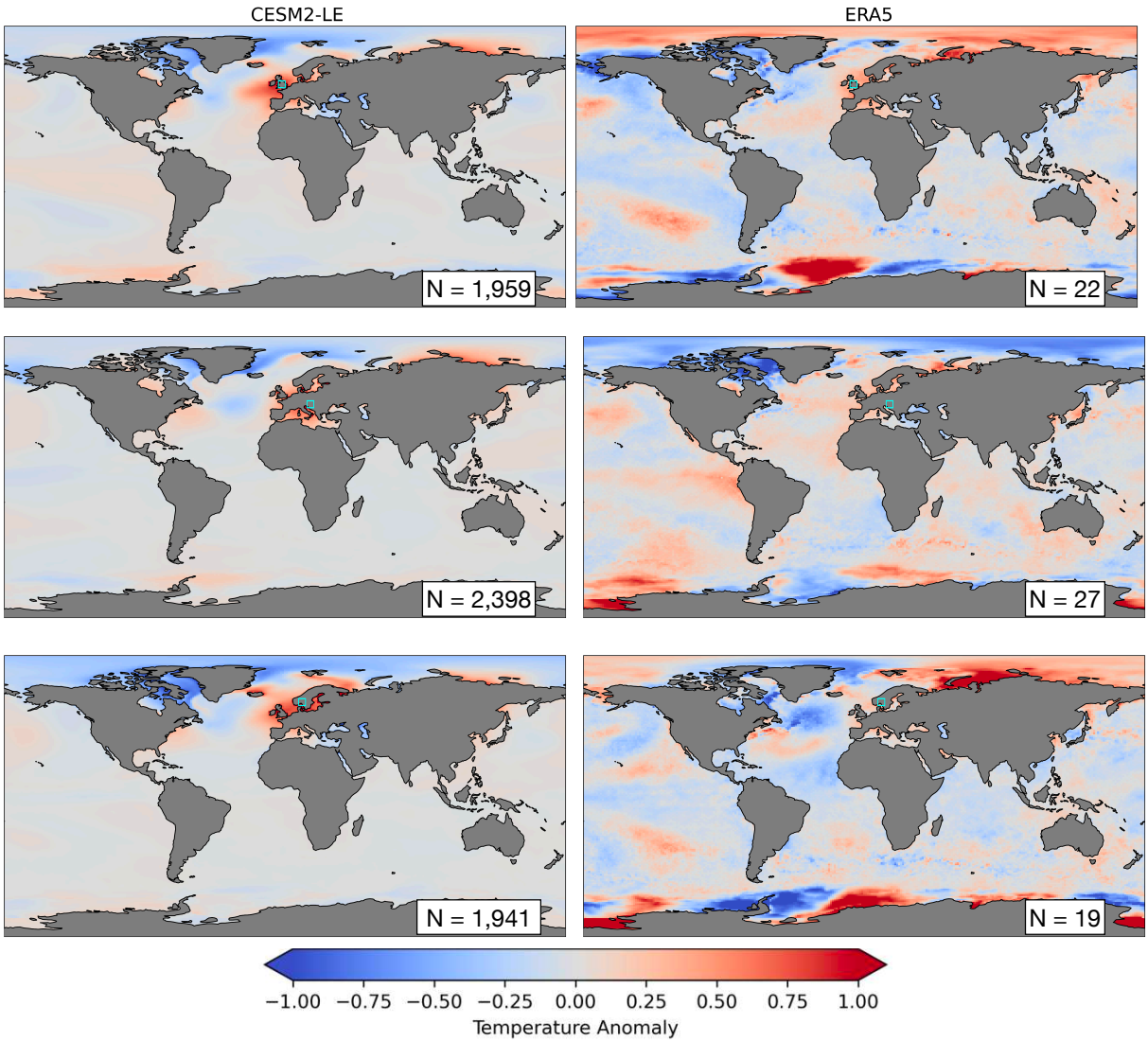


**Figure A.2:** As in Figure 2 but for central United Kingdom (52.3 N, 2.5 W), Hungary (46.65 N, 16.25 E), and eastern Norway (59.84 N 11.25 E).

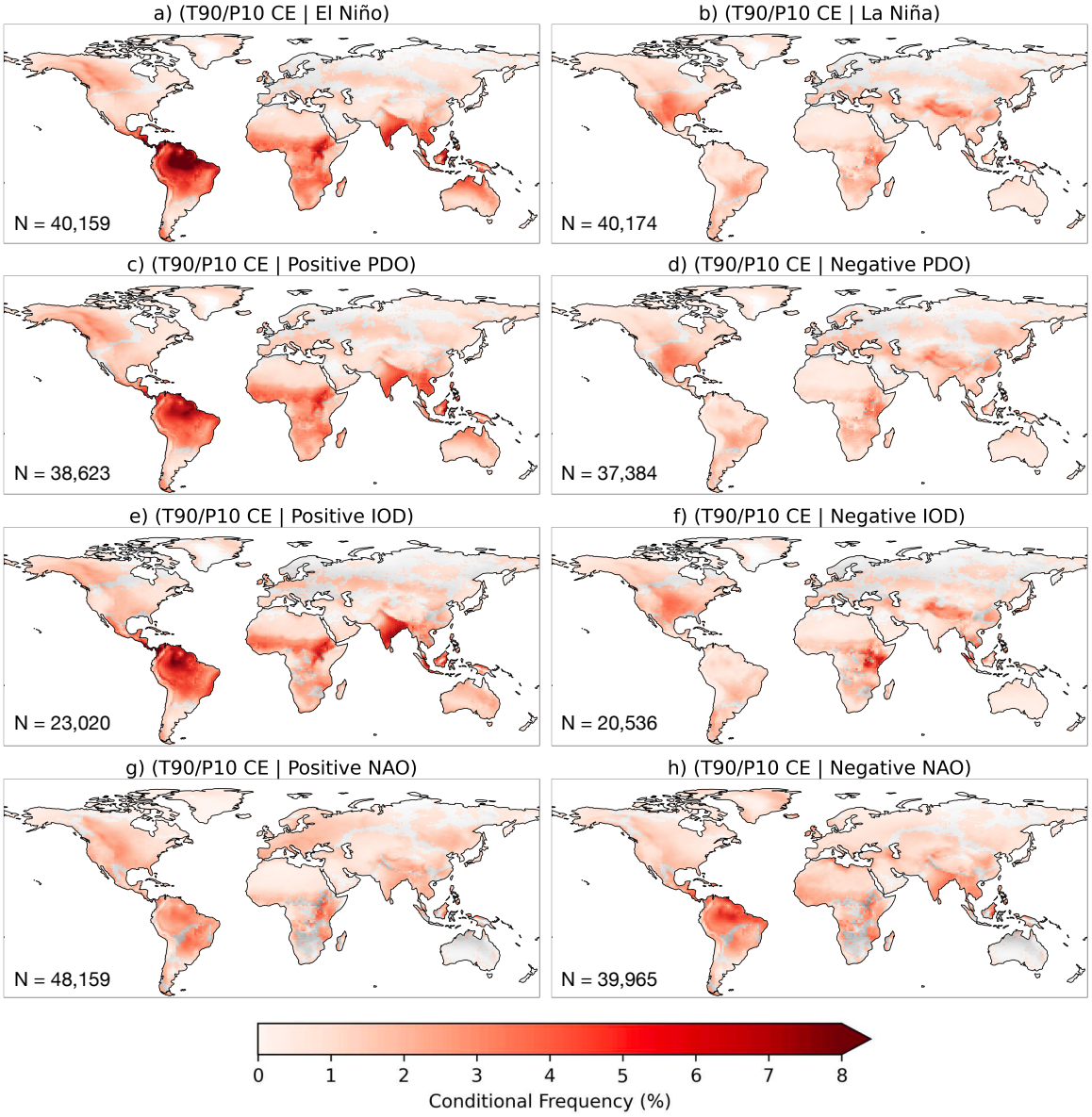


**Figure A.3:** As in Figure 3 but for one mode in each conditional.

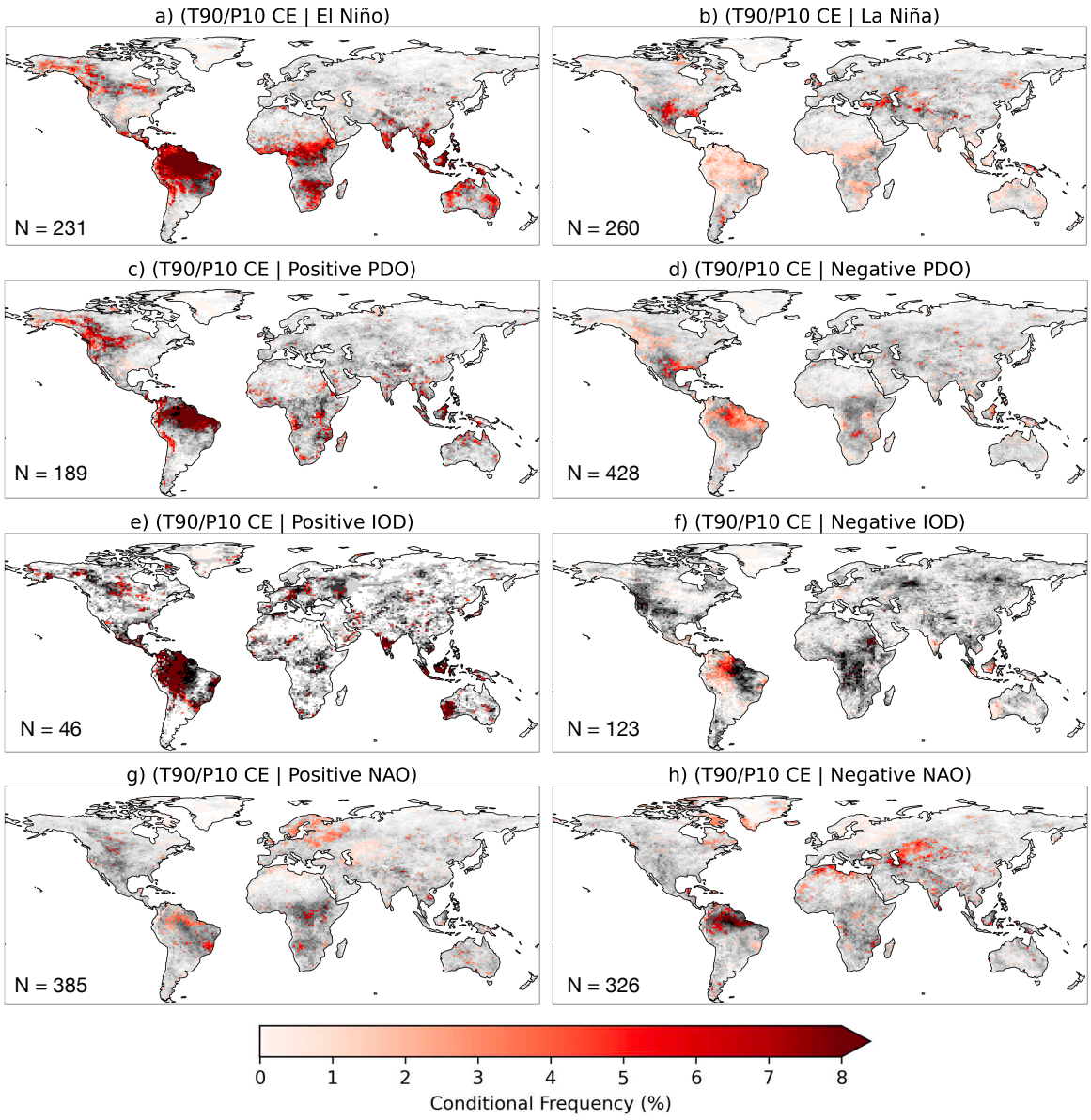


**Figure A.4:** As in Figure 4 but for one mode in each conditional.

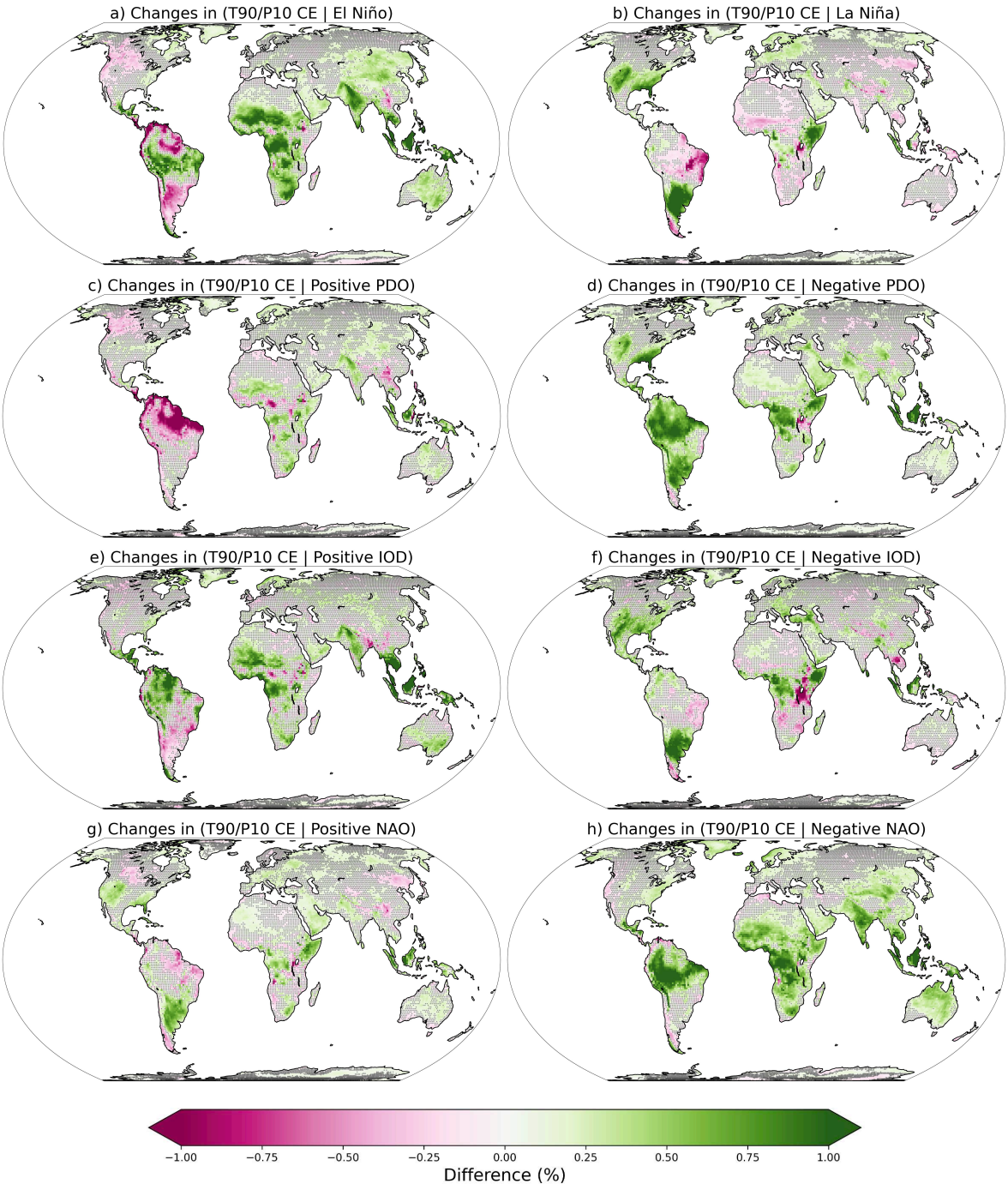


**Figure A.5:** As in Figure 5 but for one mode in each conditional.

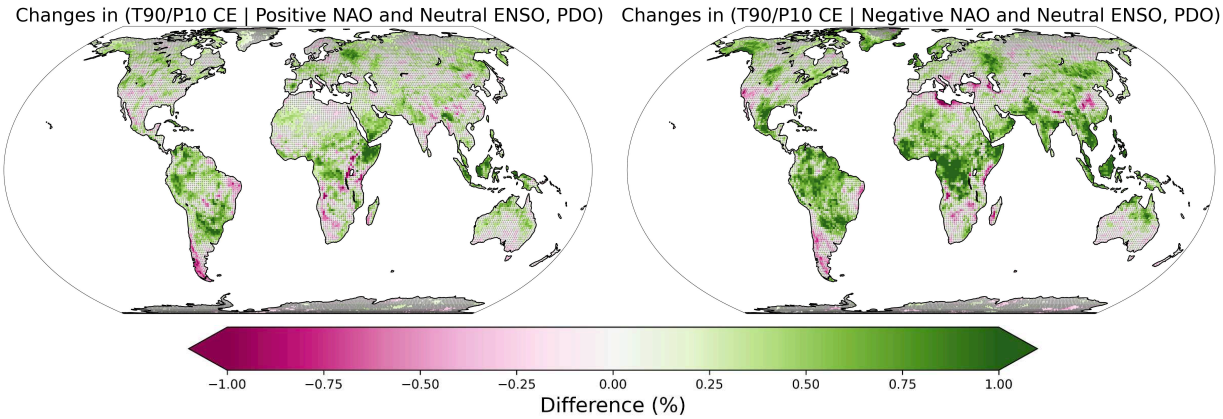


**Figure A.6:** As in Figure 5g, h but for neutral PDO and ENSO phases.

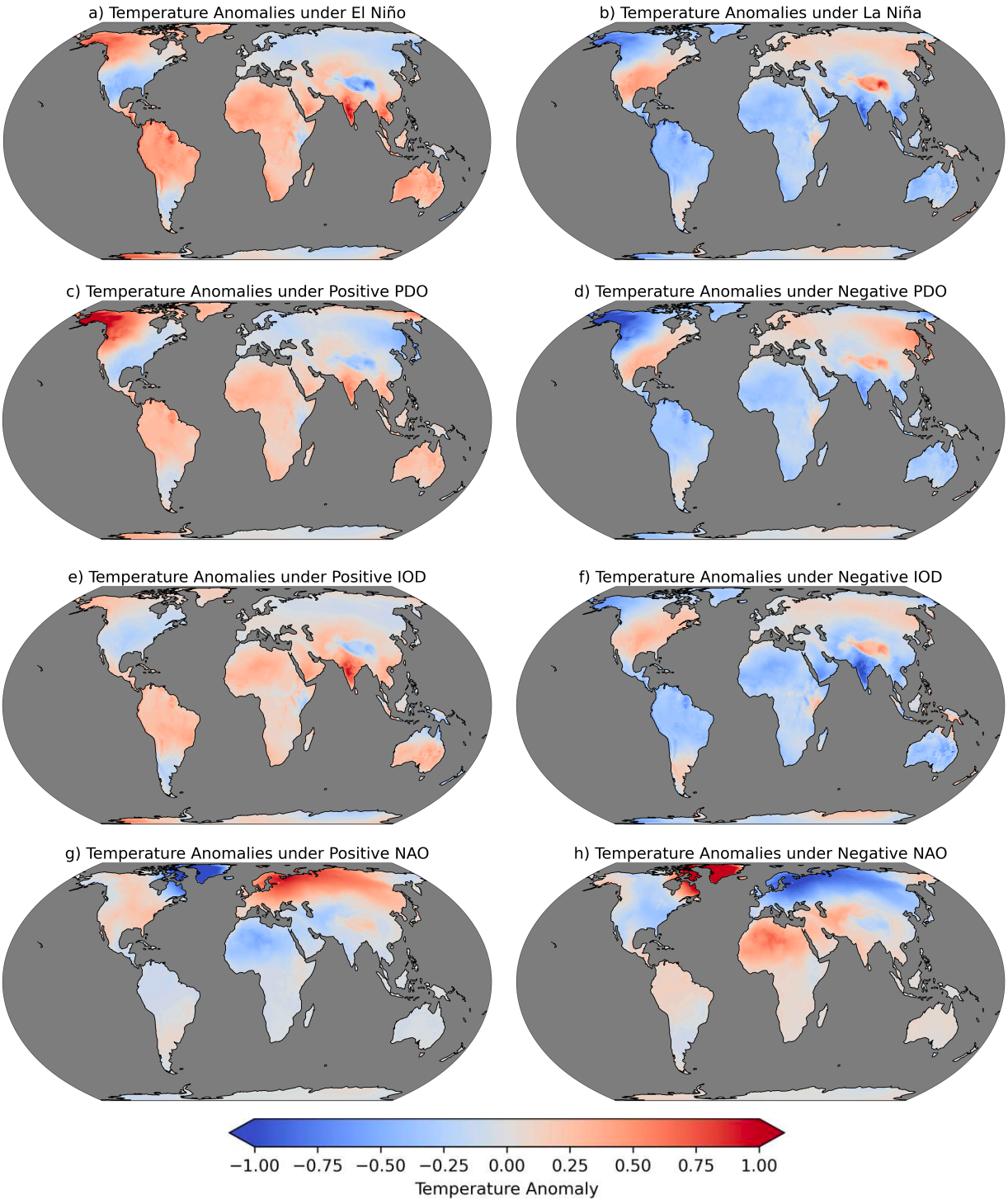


**Figure A.7:** Mean surface temperatures for all months that contain the specific climate mode phase.

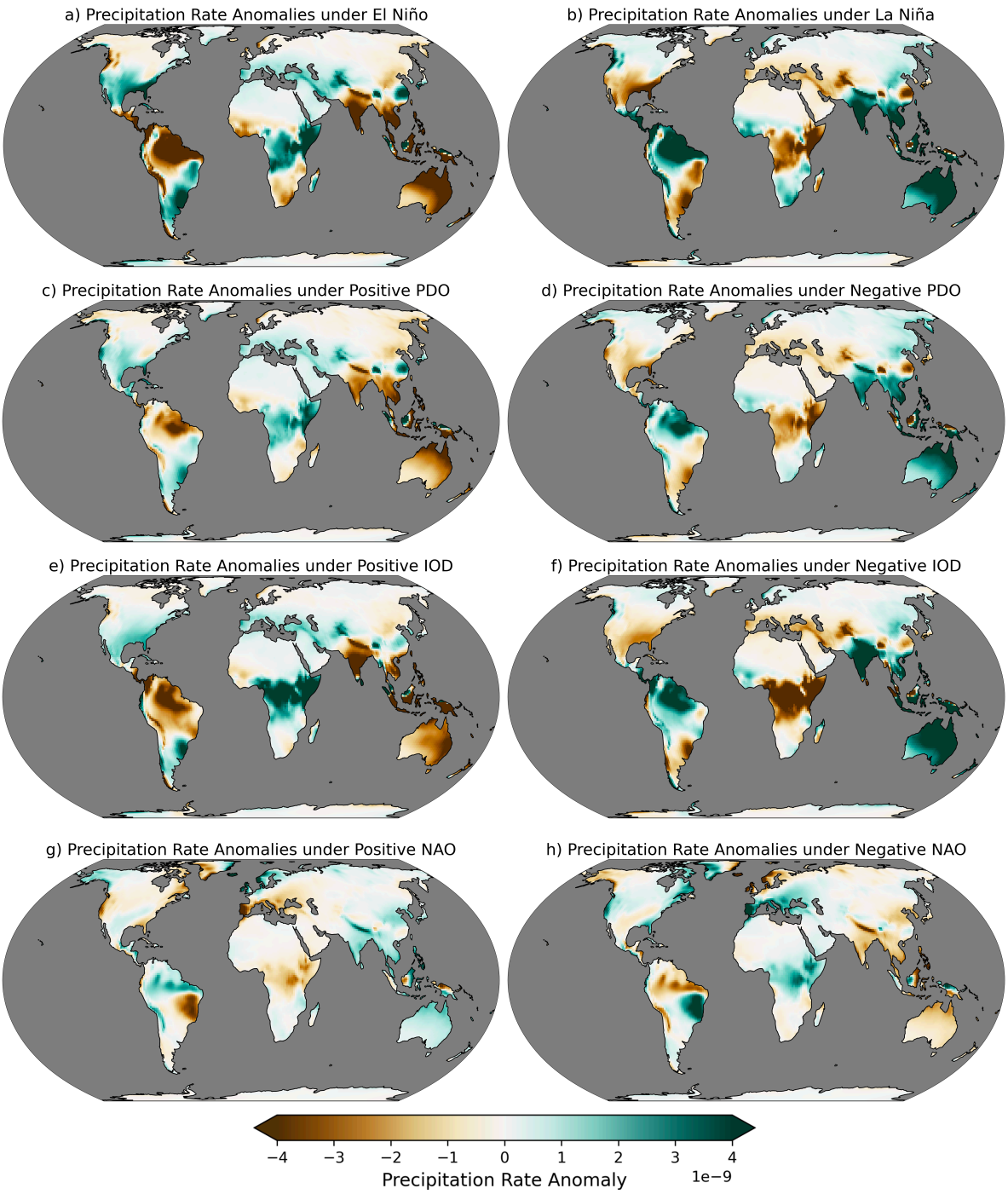


**Figure A.8:** As in Figure A.7 but for precipitation rate anomalies.

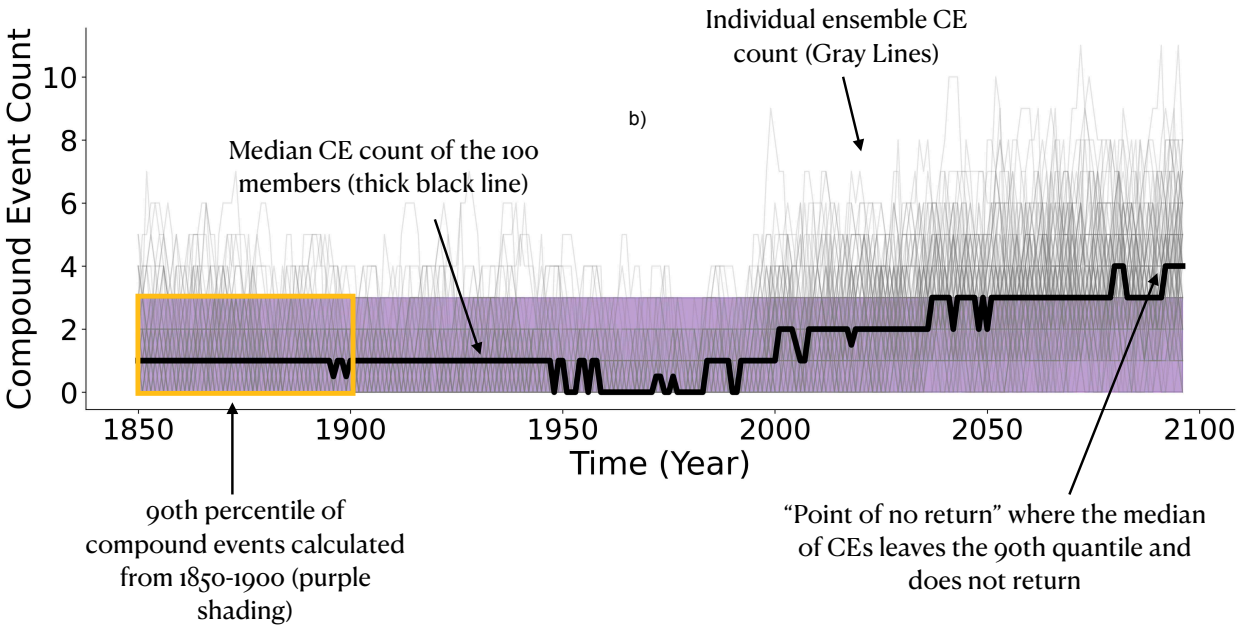


**Figure A.9:** Annotated schematic of the calculation of time of emergence in Figure 6b-g.

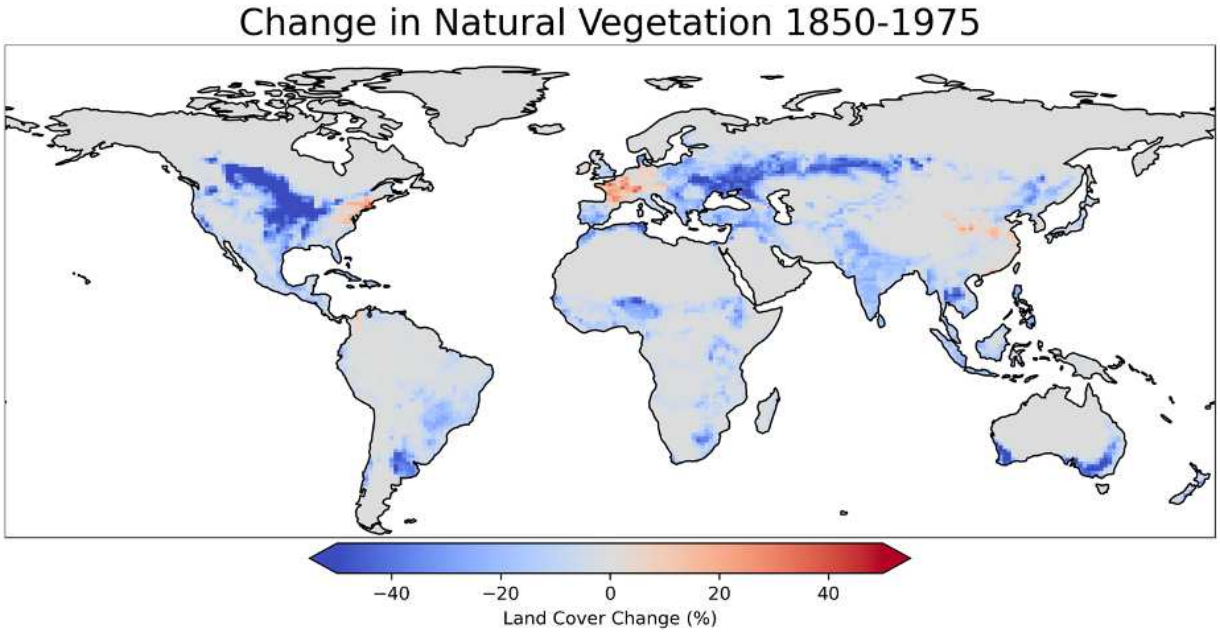


**Figure A.10:** Changes in natural vegetation in the Community Land Model in CESM2-LE for years 1850-1975. Blue indicates a decrease in natural vegetation and red indicates an increase in natural vegetation coverage.

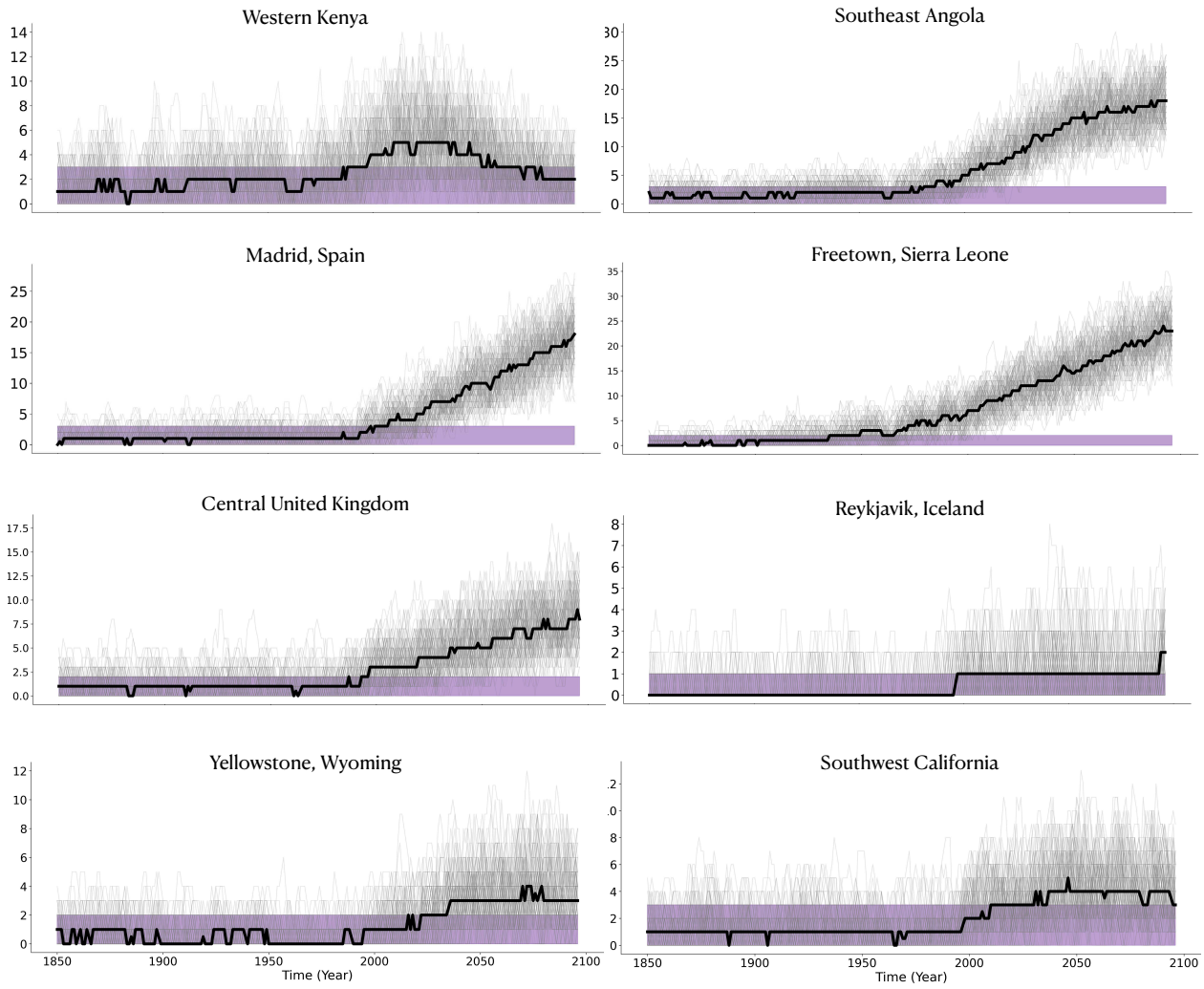


**Figure A.11:** As in Figure 6b-g but for locations over western Kenya (0.50 S, 35 E), southeast Angola (15.55 S, 21.25 E), Madrid, Spain (40.05 N, 3.8 W), Freetown, Sierra Leone (8.95 N, 13.8 W), central United Kingdom (52.90, 1.75 E), Reykjavik, Iceland (64.55 N, 22.5 W), Yellowstone, Wyoming (44.76 N, 111.2 W), and southwest California (35.34 N, 121.2 W).

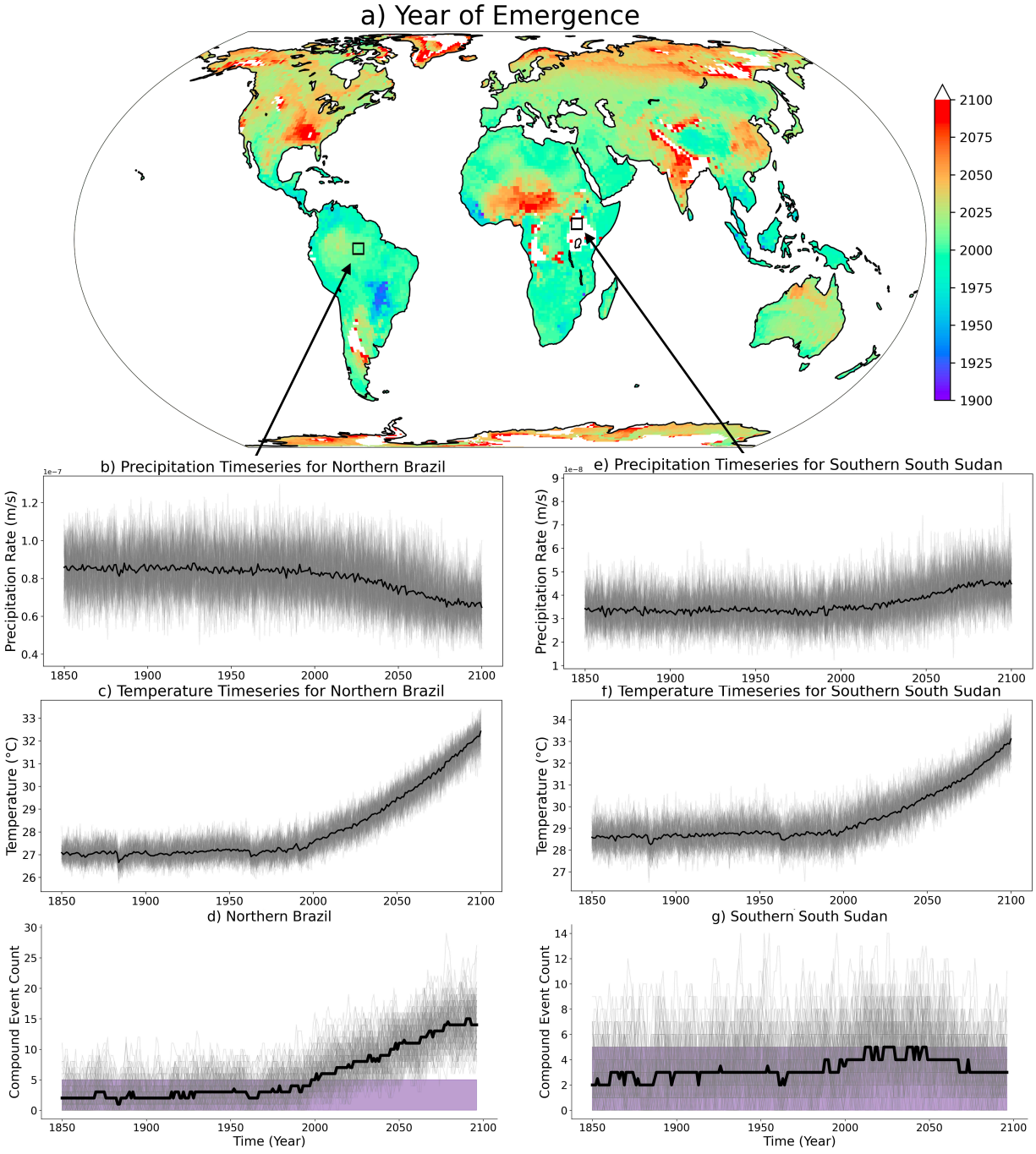


**Figure A.12:** Precipitation, temperature, and time of emergence timeseries for grid cells over northeast Brazil (3.298 S, 60 W) and southern South Sudan (5.183 N, 32.50 E).

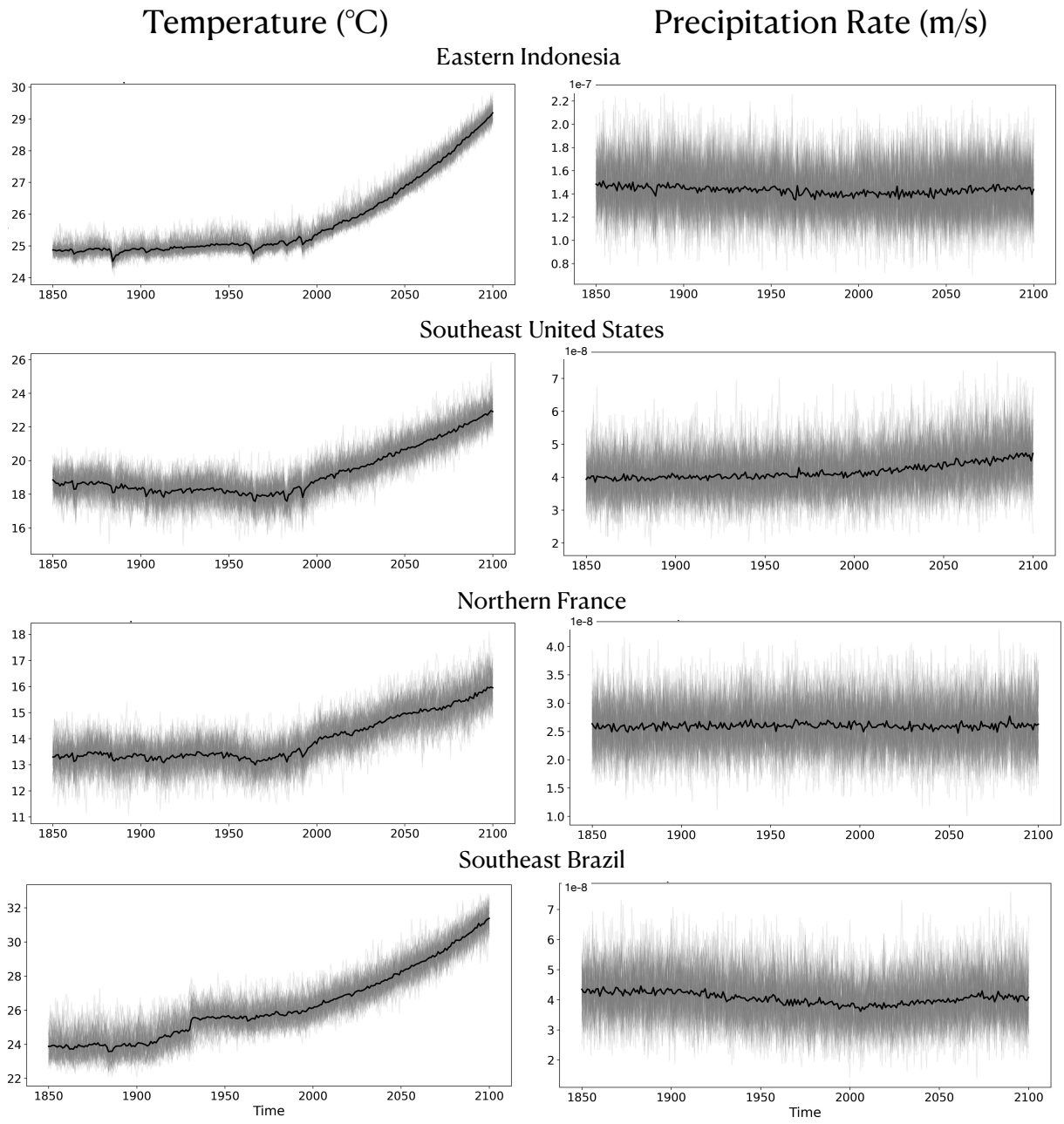


**Figure A.13:** Precipitation and temperature timeseries for grid cells over eastern Indonesia (0.47 S, 113.80 E), southeast United States (35.34 N, 88.80 W), northern France (48.53 N, 2.50 W), and southeast Brazil (20.26 S, 51.20 W).

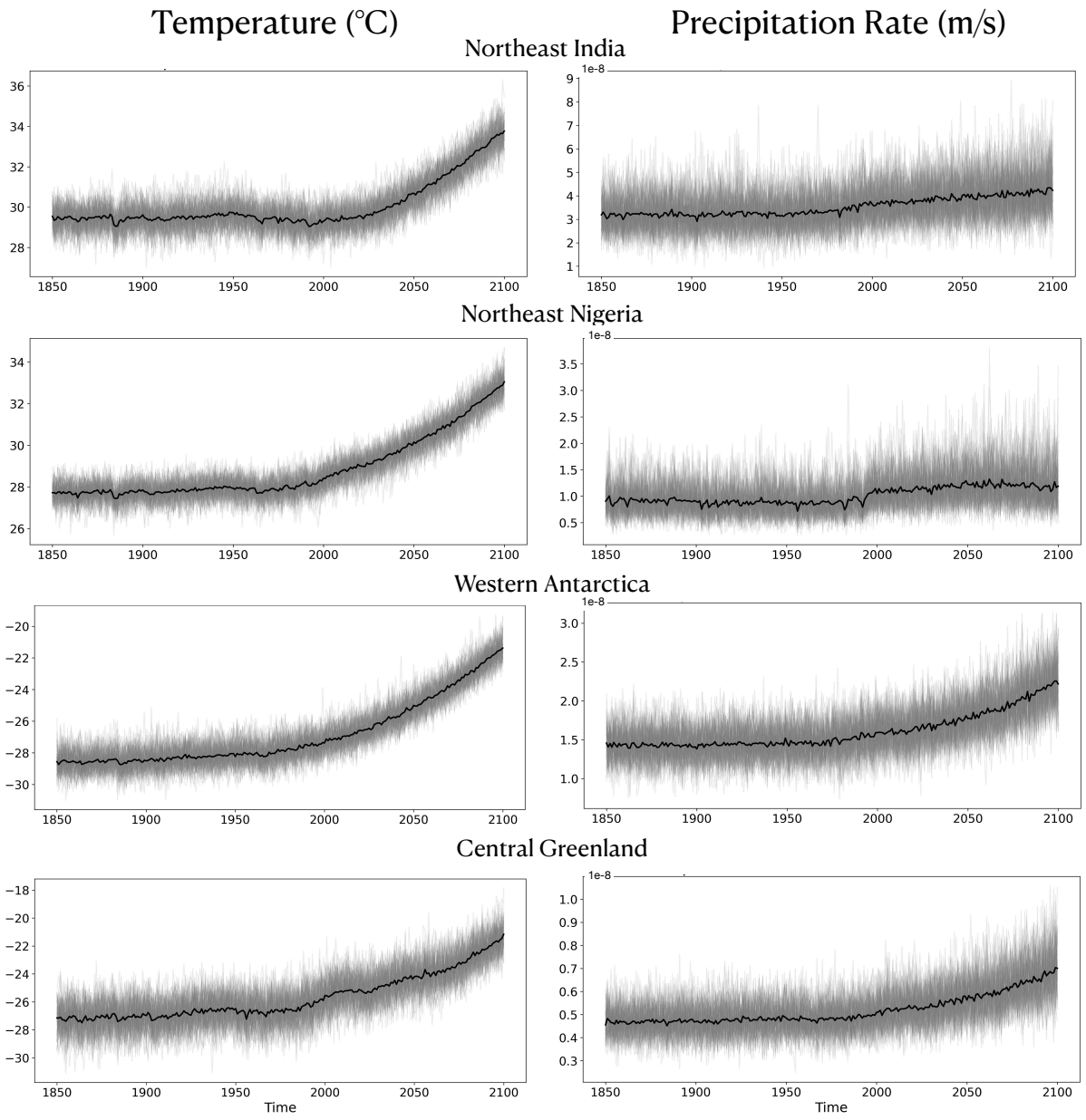


**Figure A.14:** Precipitation and temperature timeseries for grid cells over northeast India (24.03 N, 87.50 E), northeast Nigeria (12.72 N, 13.75 E), western Antarctica (76.81 S, 80 W), and central Greenland (75.86 N, 40 W).

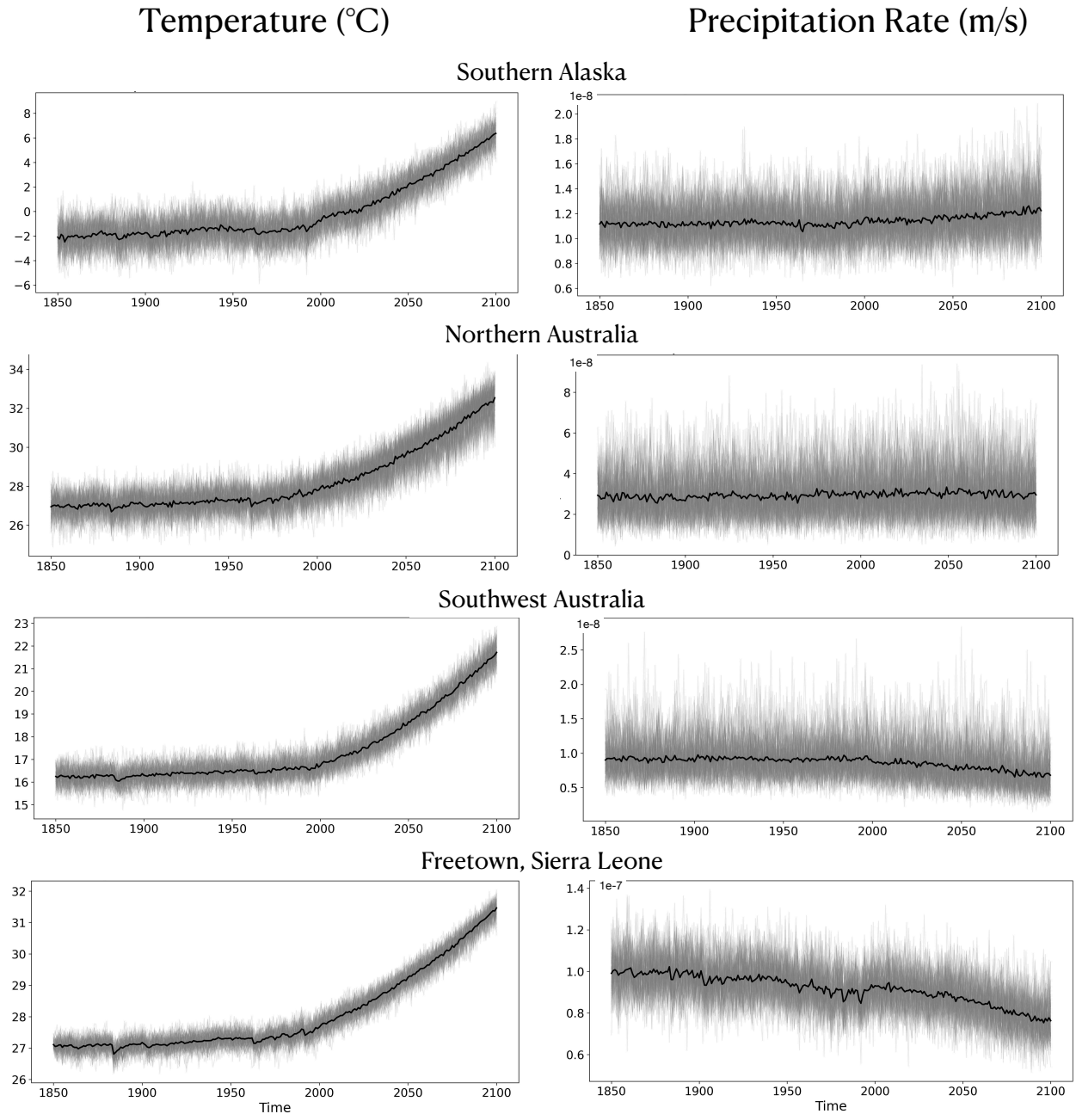


**Figure A.15:** Precipitation and temperature timeseries for grid cells over southern Alaska (60.79 N, 113.8 W), northern Australia (15.55 S, 126.2 E), southwest Australia (32.51 S, 118.8 E), and Freetown, Sierra Leone (8.95 N, 13.8 W).